## Title

Electrocorticography-based neurotechnology development: Recording from and effectively stimulating the human brain



## Author

Muller, Leah

## Publication Date

2017

Peer reviewed|Thesis/dissertation

# Electrocorticography-based neurotechnology development: Recording from and effectively stimulating the human brain

by

Leah Muller

DISSERTATION

Submitted in partial satisfaction of the requirements for the degree of

DOCTOR OF PHILOSOPHY

in

Bioengineering

in the

GRADUATE DIVISION

of the

UNIVERSITY OF CALIFORNIA, SAN FRANCISCO

AND

UNIVERSITY OF CALIFORNIA, BERKELEY

Acknowledgments

I would like to thank my advisor, Dr. Edward Chang, for the opportunities, and my committee, Drs. Michel Maharbiz, Daniel Lowenstein, and Loren Frank, for the ongoing advice and encouragement.

I would also like to thank my family and friends for their ongoing encouragement in this long journey.

Some material presented in this work is published in peer-reviewed journals:

Leah Muller, Liberty S. Hamilton, Erik Edwards, Kristofer E. Bouchard, and Edward F. Chang. Spatial resolution dependence on spectral frequency in human speech cortex electrocorticography. Published in Journal of Neural Engineering, 2016.

Leah Muller, Sarah Felix, Kedar G. Shah, Kye Lee, Satinderpall Pannu, and Edward F. Chang. Thin-film, high-density micro-electrocorticographic decoding of a human cortical gyrus. Published in IEEE, 2016.

Electrocorticography-based neurotechnology development:

Recording from and effectively stimulating the human brain

Leah Muller

Neural devices have great potential to improve the treatment of neuropsychiatric, sensorimotor, and epileptiform disorders in humans. Recently, focus has been appropriately directed toward enabling the bidirectional flow of information between these devices and the brain with the goal of delivering electrical therapy only when necessary and in an appropriate amount. Interactions between the nervous system and the device improve when the devices are able to 1) record high quality neural signals using the appropriate number of sensors over the correct area and 2) stimulate the brain with an electrical signal that causes a desired effect.

The work presented here addresses these two major issues necessary for neural device design. In the first section, the spatial resolution of the brain at its surface is investigated and quantified using recordings from human patients with implanted ECoG sensors. In the second section, a novel ECoG sensor array with high spatial resolution is described and tested in human subjects that undergo awake brain surgery. Finally, the neural changes associated with sub-threshold and super-threshold electrical stimulation are examined and described for the first time in relation to stimulation parameters and stimulation outcome.

We found that the level of spatial resolution at the cortical surface depends on the neural frequency. For the highest neural frequency studied, the high gamma band, a

denser array of sensors than what is commercially available should increase the information content. Because of this observation, we worked with Lawrence Livermore National Labs to manufacture an array of electrodes for collecting neural activity from a single human gyrus, and we observed that the increased density of electrodes did indeed improve decoding accuracy. Electrical stimulation of the sensorimotor cortex induced high gamma activity when the subject consciously perceived the stimulation, suggesting that high gamma is a reliable biomarker of effective stimulation. Together, these results suggest that devices should record from the brain's surface at a higher density than is typically used, and that high gamma can be utilized as a feedback signal indicating whether stimulation is effective.

Table of Contents

List of Figures

Chapter 1



Chapter 2



Chapter 3

# Introduction

In the last half a century, the fields of biomedical engineering, electrical engineering, mechanical engineering, and neuroscience have fostered the development of devices that interface with the nervous system. For humans, neural devices restore basic senses (cochlear and retinal implants), alleviate pain (i.e., spinal cord stimulation), and provide therapy for neural disorders such as Parkinson's disease and epilepsy (deep brain stimulation, cortical stimulation, and vagal nerve stimulation), among many other indications. In all of these examples, the devices are based on the same principle: electrodes placed in an appropriate area of the nervous system send electrical impulses, and the nervous system alters its activity based on this artificial input.

Electrocorticography (ECoG) is the recording of neural activity from the surface of the brain. With ECoG, a large area of the cortical surface may be monitored at relatively high spatial resolution and high temporal resolution. The large spatial coverage is in contrast to penetrating arrays that cover at most a couple of square centimeters of the cortical surface; ECoG can cover hundreds of square centimeters. On the other end of the spectrum is EEG, which records from the scalp; in comparison, ECoG achieves drastically higher spatial resolution and attains higher signal quality due to its direct placement on the cortical surface. Finally, temporal resolution is achieved because ECoG is an electrical measurement with little time lag, in contrast to methods such as fMRI. From a safety standpoint, ECoG has the benefit of not penetrating brain tissue, thus reducing tissue damage and inflammation. Tissue damage and resulting gliosis, such as is caused by insertion of electrodes into the cortex, is associated with

loss of signal over time, a complication that ECoG avoids. Finally, because ECoG-based devices have the potential to be implanted, they can record from the brain for long-term applications.

In recent years, focus has been directed toward enabling the bidirectional flow of information to enhance the capabilities of neural devices. In this paradigm, referred to as ‘closed-loop stimulation,’ neural devices receive information from the nervous system and use it to inform the way that they deliver electrical pulses. Interactions between the nervous system and the device improve when the devices are able to 1) record high quality neural signals using the appropriate number of sensors over the correct area and 2) stimulate with an electrical signal that induces beneficial neural modulation in that area.

The work presented in the following pages addresses these two major issues necessary for neural device design. In the first section, the spatial resolution of the brain at its surface is investigated and quantified using recordings from human patients with implanted ECoG sensors. In the second section, a new kind of ECoG sensor array with even higher spatial resolution is described and tested in human subjects that undergo awake brain surgery. Finally, the neural changes associated with sub-threshold and super-threshold stimulation are examined and described for the first time in relation to stimulation parameters and stimulation outcome.

# Spatial resolution dependence on spectral frequency in human speech cortex electrocorticography

**Leah Muller[1,2,3], Liberty S. Hamilton[1,4], Erik Edwards[1,4], Kristofer E. Bouchard, and Edward F. Chang[1,4]**

[1]Department of Neurological Surgery and Department of Physiology, University of California, San Francisco, 675 Nelson Rising Lane, Room 511, San Francisco, CA 94158, USA, [2]Joint Program in Bioengineering, UC Berkeley/UC San Francisco, [3]Medical Scientist Training Program, UC San Francisco, [4]Center for Integrative Neuroscience, University of California, San Francisco, San Francisco, CA

Email: edward.chang@ucsf.edu

**Abstract** *Objective*. Electrocorticography (ECoG) has become an important tool in human neuroscience and has tremendous potential for emerging applications in neural interface technology. Electrode array design parameters are outstanding issues for both research and clinical applications, and these parameters depend critically on the nature of the neural signals to be recorded. Here, we investigate the functional spatial resolution of neural signals recorded at the human cortical surface. We empirically derive spatial spread functions to quantify the shared neural activity for each frequency band of the electrocorticogram. *Approach*. Five subjects with high-density (4mm center-to-center

spacing) ECoG grid implants participated in speech perception and production tasks while neural activity was recorded from the speech cortex, including superior temporal gyrus, precentral gyrus, and postcentral gyrus. The cortical surface field potential was decomposed into traditional EEG frequency bands. Signal similarity between electrode pairs for each frequency band was quantified using a Pearson correlation coefficient. *Main results*. The correlation of neural activity between electrode pairs was inversely related to the distance between the electrodes; this relationship was used to quantify spatial falloff functions for cortical subdomains. As expected, lower frequencies remained correlated over larger distances than higher frequencies. However, both the envelope and phase of gamma and high gamma frequencies (30-150Hz) are largely uncorrelated (<90%) at 4mm, the smallest spacing of the high-density arrays. Thus, ECoG arrays smaller than 4mm have significant promise for increasing signal resolution at high frequencies, whereas less additional gain is achieved for lower frequencies. *Significance.* Our findings quantitatively demonstrate the dependence of ECoG spatial resolution on the neural frequency of interest. We demonstrate that this relationship is consistent across patients and across cortical areas during activity.

**Keywords:** electrocorticography, brain machine interface, neural device design, spatial resolution, neural frequency band

## 1. Introduction

Electrocorticography (ECoG) is a method of recording electrical neural signals from the cortical surface and is a well-established clinical tool for localizing seizure foci in epileptic patients. Clinical ECoG records neural activity using electrodes positioned in a grid arrangement, usually spaced 1cm apart. More recently ECoG has found utility in both scientific and engineering applications due to its high spatial and temporal resolution relative to noninvasive imaging

approaches. In research applications, high frequency neural responses have been shown to be informative for task-related neural decoding, while low frequency bands can serve as markers for neural states (N. E. Crone, Korzeniewska, & Franaszczuk, 2011; Engel & Fries, 2010; Fries, Nikolić, & Singer, 2007; Kellis et al., 2010; Lachaux, Axmacher, Mormann, Halgren, & Crone, 2012; Miller et al., 2007; Ray, Crone, Niebur, Franaszczuk, & Hsiao, 2008; Womelsdorf & Fries, 2007). Moreover, high frequency neural signals have been described to be more spatially discrete than low frequency signals(Buzsaki & Draguhn, 2004; Edwards et al., 2009; Leski, Lindén, Tetzlaff, Pettersen, & Einevoll, 2013; Pesaran, 2010; Viventi et al., 2011). However, the spatial resolution of neural signals from the human cortical surface with respect to these functional neural frequency bands has never been fully quantified in humans.

Higher density ECoG grids collect more information from the cortical surface than the standard 1 cm grids, leading to better decoding performance in brain machine interface applications(Blakely, Miller, Rao, Holmes, & Ojemann, 2008; Breshears et al., 2011; Flinker, Chang, Barbaro, Berger, & Knight, 2011; Kellis et al., 2010; Khodagholy et al., 2015; Leuthardt, Freudenberg, Bundy, & Roland, 2009; Wang et al., 2009). In most cases, these high density arrays have covered a very small area of cortex, and therefore large scale comparisons of shared signal in space have not been evaluated. Recently, correlations in the raw signal have been explored with respect to distance using a clinical ECoG array and a microwire ECoG array(Kellis et al., 2015). However, the measured signals from the microwire array are inherently different from those of the clinical array due to filtering effects of electrode size and shape(Kent & Grill, 2014; Lempka et al., 2011). Furthermore, the microwire array can examine signal similarity only within a very small area of cortex, while the clinical array sparsely samples a wide expanse of cortex that may or may not be actively engaged at the time of recording.

Ultra high-density, low impedance electrode arrays for chronic human recordings are not

presently FDA approved in the United States, which is a dilemma for empirically deriving spatial resolution values for this work. Work in animal models can give us some insight into spatial correlations at higher electrode density(Kajikawa & Schroeder, 2011; Katzner et al., 2009; Xing, Yeh, & Shapley, 2009); however, it may be that spatial correlations in human cortex differ due to differences in underlying cytoarchitecture, cortical thickness, and differences in cortical folding across species(Elston, 2003). Thus, we hope that this study serves to illustrate the utility of moving toward higher-density arrays in human subjects as well. A high-density ECoG grid with 4mm spacing of electrodes offers a unique opportunity to identify shared signal at close spacing of electrodes, over a broad area of active cortex, and across neural frequency bands. We describe frequency band-specific spatial spread at the cortical surface in patients performing speech-related tasks. We use these observations to compare spatial spread functions across patients and across functional areas during speech perception and production tasks.

## 2. Materials and Methods

### *2.1 Experimental setup*

*2.1.1. Subjects* Experimental procedures were approved by the Committee for Human Research at the University of California, San Francisco, and all participants provided written informed consent. Patients undergoing ECoG grid implantation for epilepsy focus localization (N=5, 0M/5F, 25 – 41 years old) volunteered to participate in this research study. Patients were implanted with 256 channel high-density subdural electrode arrays (AdTech, Racine, WI or Integra, Plainsboro, NJ) with 4mm center-to-center spacing (1.17mm exposed diameter). Electrodes were positioned according to clinical criteria but included coverage over the superior temporal gyrus and the ventral sensorimotor cortex (pre- and post-central gyri). An electrode in the sub-galeal space served as the reference electrode and ground.

*2.1.2. Tasks and stimuli* The patients either spoke or listened to sentences taken from the TIMIT database (Garofolo, 1993; Wrench, 1999). In the listening task, patients heard a subset of 125 sentences drawn pseudo-randomly from a list of 499 sentences spoken by 354 male and 145 female speakers. In the speaking task, patients were instructed to read a set of 50 sentences, presented visually on a laptop screen at a user-driven pace. In both tasks, sentences were chosen to evenly sample the distribution of phonemes present in English. These tasks lasted approximately 5-10 minutes each. Presentation of experimental stimuli was synchronized to neural recordings and controlled using custom MATLAB software running on a Windows laptop.

*2.2 Recording and data processing*

Signals were acquired at a sampling rate of 3051.8 Hz and were amplified and digitized using a Tucker-Davis Technologies (Alachua, FL, USA) neural recording system (RZ2 DSP combined with a 256-channel PZ2 amplifier). Manual artifact and channel rejection was performed, followed by common average referencing (CAR) (N. Crone, Boatman, Gordon, & Hao, 2001). The CAR consists of the mean across sixteen-channel banks of non-rejected electrodes that are spatially arranged in a row that spans 6cm. The CAR approximates the activity contributed by the original reference, so subtracting the CAR from each channel largely removes contributions of the original reference electrode and electrical artifacts that are often present in groups of sixteen channels due to shared connectors and cabling (see Crone et al. 2001 for a discussion of CAR in ECoG recordings). The CAR can also be thought of as the spatial DC portion of the signal, and CAR-re-referencing as a typical mean or DC removal.

The signal from each electrode channel was filtered into 40 frequency bands using an FFT followed by a Hilbert transform with logarithmically increasing center frequencies (range of CF = 4.07 Hz – 193.8 Hz). The analytic amplitude, also known as the envelope, and the phase were calculated for each (Edwards et al., 2009). The filtered frequencies were then averaged into

frequency bands corresponding to the traditional theta (4 – 7 Hz), alpha (7 – 14 Hz), beta (15 – 30 Hz), gamma (30 – 60 Hz), and high gamma (70 – 150 Hz) bands. This signal was then z-scored with respect to rest (no-task) epochs within the same recording. The anatomical location of electrodes was determined with the aid of co-registered brain CT and MRI images. The precentral gyrus (preCG), the postcentral gyrus (postCG), the suprasylvian region, the superior temporal gyrus (STG), and the middle temporal gyrus (MTG) were grouped and evaluated separately for some analyses.

*2.3 Analytical methods*

Electrodes were chosen for analysis within an anatomically defined area using a bootstrap t-test to find electrodes that responded significantly to speech over silence in the high gamma band. The high gamma band was chosen because it has been shown to exhibit specificity in activation to speech sounds in eloquent cortex. Electrode responses during speech were compared to responses during silence using short consonant-vowel syllables as the stimulus. The threshold p-value for inclusion was $p<0.001$ over 10,000 bootstrap iterations. Of the 256 electrodes on the grid, an average of 80±6 electrodes were anatomically localized to the superior temporal gyrus, which is expected to respond to speech sounds. Of these anatomically localized electrodes, an average of 87% showed significant responses to speech over silence.

A Pearson correlation coefficient was calculated between the time series of either the analytic amplitude or the phase of each electrode pair within the anatomically and functionally defined subset (described above) and associated with the Euclidean distance between the electrodes. Figure 1 shows representative data along with its subsequent comparison for two nearby electrodes. For simplicity, the term ‘component’ will be used to refer to either the analytic amplitude or the phase of a single frequency band for a single patient. The entire 5-10 minutes of data from each task were used to derive the correlation coefficient for the aforementioned

subsets of electrode pairs. Both the electrode subset and the time series used to derive correlation coefficients varied by task. The datasets for the two tasks were analyzed independently. We calculated chance level correlations for each frequency band by randomizing the data for each component in time for each electrode separately and repeating the correlation measures for all distances. Correlations for the randomized data fell very close to zero (± $5x10^{-4}$) irrespective of frequency band and distance.

To define the spatial relationship of correlation between electrode pairs, we modeled the falloff of the electrode correlations vs. distance, using the interquartile range of the data for each component. We tested exponential (equation 1), Lorentzian (equation 2), Gaussian (equation 3), and power law (equation 4) functions to describe this falloff. These equations were chosen to fit the data because they are typical equations that describe non-linear fall offs and that allow for the necessary observation that when distance is zero, correlation is one. A constant term was added where necessary to correct for the noise floor of the correlation dataset, which is most likely due to either shared activity from the reference electrode or shared noise (Bruns, Eckhorn, Jokeit, & Ebner, 2000). In each case, the number of free parameters was limited to two to avoid over-fitting of the function to the data.

$$y = (1 - c)e^{-Bx} + c \quad (1)$$

$$y = (1 - c)\frac{B^2}{B^2 + x^2} + c \quad (2)$$

$$y = (1 - c)\frac{e^{-x^2}}{B} + c \quad (3)$$

$$y = (x + 1)^{-B} \quad (4)$$

These functions were fit separately for each component, allowing maximum goodness of fit and

equal opportunity for different functions to describe the different frequencies. The best-fit equation was chosen as the one with the highest R-squared value using a least-squares method. For each component, the best-fit function across patients was chosen to represent the average falloff of correlation versus distance. To adequately capture the curvature of the falloff, we used only pairwise correlations at distances of 20mm and below. Using data in this range minimizes the contribution to the fit from the noise floor of low correlation, which is also captured in the constant *c*. The fits with the highest R-squared values were corroborated by visual inspection; the data were well approximated by the chosen fit for every patient at every frequency.

**3. Results**

The goal of our study was to quantify the average spatial spread at the cortical surface for each functional frequency band. Using high-density ECoG arrays and data from human intracranial recordings, we applied a correlation-based analysis to determine the extent of shared signal across the cortical surface for the amplitude and phase content of five frequency bands.

A natural starting point for estimating spatial falloff is to look at that of the raw signal before decomposing the signal into frequency bands. This is shown in Figure 2, where for each distance of separation on the electrode grid, the interquartile range of data points is plotted as a box plot. The majority of electrode pairs are correlated above noise floor only within 2cm; after this distance of separation between electrodes the plot approximates a horizontal line. Therefore, only electrodes located 2cm or less from one another were used for analyses. We then fit curves to the data points corresponding to electrode pair correlations to describe the falloff of correlation with distance. The best fit in this example is plotted with a dashed line. Note that the curve continues to points that are unobservable by the high-density grid, including distances less that 4mm. This part of the curve is extrapolated, and it can give us intuition about

what correlations would be observed in the raw signal with more closely spaced electrodes, with the caveat that correlations at distances below 1.17mm (the contact diameter of the electrode) are underestimated.

Correlations at low frequencies are higher in magnitude and more widespread than at high frequencies. This is shown in Figure 3 for the theta and the high gamma frequency bands. The high gamma band signals at nearby electrodes show a lower maximum correlation in comparison to the theta band signals, and the spatial spread of notable correlations encompasses less area on the cortical surface than that of theta. As expected, we observe a decrease in correlation between pairs of electrodes as the distance increases between them.

The correlations between electrode pairs differ predictably not only by frequency band but also by whether or not the patient was engaged in a task. The tasks that we examined were speech perception and production. The rest versus task distinction is particularly evident in the high gamma band for electrodes that are considered active (see Methods for details in determining which are active). Figure 4 shows the drastic difference in correlation patterns with distance for electrodes in the STG when the patient listened to speech versus when the patient sat quietly. Points at each distance are represented in a distribution plot to compare the shape of distributions. The correlations are more variable and on average higher during rest than when the patient is listening to speech. Both the median and the mean are lower during activity than during rest at all distances. A paired t-test was performed for the correlation values at each distance, and at all distances shown (distance<20mm) there were statistically significant differences in correlations for task vs. rest ($p<0.05$). Similar differences in correlation with activity have been described elsewhere (Buckner & Vincent, 2007; Cohen & Kohn, 2011; Fukushima, Saunders, Leopold, Mishkin, & Averbeck, 2012). Because correlations decrease with activity, the spatial spread function shows a steeper fall off during activity than during rest.

Considering this fact, and additionally considering that the neural signal of interest is most likely elicited while a subject is engaged in a task of some sort, we decided to base the remainder of our analyses on electrodes that are considered active in an anatomical area, during a stimulus that elicits that activity.

As mentioned in Section 2.3, four functions were fit to the data. Representative data from the theta band of one subject is shown with all fit lines superimposed in Figure 5. The Lorentzian and exponential forms were similar in shape and in goodness-of-fit, and the R-squared value for goodness-of-fit was quite high for both ($R^2_{Lorentzian}$ = 0.93, $R^2_{exponential}$ = 0.92). Indeed, the best fit choice was either Lorentzian or exponential for all components tested; however, the difference between $R^2$ values for these models increased for high neural frequencies (gamma and high gamma). Regardless of whether the function tested was Lorentzian or exponential, the resulting fit lines for correlation decrease with distance differed only slightly. In all cases, the Lorentzian and exponential forms were greatly superior to the Gaussian and Power Law forms in describing the falloff in correlation for each component.

Across frequency bands there is a nonlinear falloff of correlation with distance for both amplitude and phase of the signal. The falloff becomes steeper as the neural frequency increases. This is shown in Figure 6 where best fits are averaged over five patients. The fits shown are for electrodes in the STG while the patients listened to sentences. There is a clear similarity in falloff pattern for theta and alpha bands and for gamma and high gamma bands. In the analytic amplitude data, correlation falloffs were best fit by a Lorentzian function in individual patients as well as the subject-pooled data. For phase correlations, theta and alpha were best fit by an exponential function, whereas beta, gamma, and high gamma were best fit by the Lorentzian. Importantly, the best fit function in each case was identical across patients. This did not have to be the case, since the analytic amplitude and phase for each frequency band for

each patient were fit separately. The functional form of best fit for any patient could have differed from that of the other patients for the same component; however, all components of the same class were fit best with the same functional form across all five patients. This made the task of defining a best fit curve for each component easy because we simply average the coefficients of best fit for each component across patients.

To determine if the form or slope of the best fit function differs by anatomical location, we then took correlations between electrodes overlying the preCG and postCG while the patient spoke sentences, a task that evokes reliable activity in the sensorimotor cortex(Bouchard, Mesgarani, Johnson, & Chang, 2013). The correlation analysis was repeated for these anatomical areas. Again we found the same effect: a steeper correlation falloff with increasing neural frequency. On closer comparison of fits between areas, we found that the spatial correlation falloff fit lines for preCG, postCG, and STG did not differ significantly ($p>0.05$, paired t-test with Bonferroni correction for multiple comparisons). Therefore, the presented results also apply to the pre- and post-central gyri as well as to the STG. This is shown in Figure 7 as a function of the coefficient B, which represents the steepness of descent of the fits. This coefficient value is conserved over patients and anatomical areas, but notably not across frequency bands. The shift in value can be noted best for the same function form for all analytic amplitude fall offs. The B values shift from a relatively high value to a lower value as frequency band increases, corresponding to the increased steepness of the fall off with distance. The same pattern is seen with best fits in the phase data.

Our estimations to this point were mostly constrained to a single gyrus and by nature assume a continuous surface. We next wanted to determine how anatomical factors such as cerebral convolutions and lobar divisions affect spatial correlations. We therefore analyzed the spatial correlations between electrodes that were within a single gyrus, across a sulcus (the superior temporal sulcus between the STG and MTG), and across brain lobes (the Sylvian Fissure,

between the frontal and temporal lobe). We hypothesized that spatial correlations within the STG would be significantly greater than across the superior temporal sulcus, and even more so than across the Sylvian Fissure. To test this prediction, we shifted our focus from the interquartile range to the upper quartile range of values so that high correlation values were preserved. We observed that correlations were higher between electrodes within a gyrus and that patterns of correlation seemed to cluster with anatomical boundaries such as sulci. This relationship was quantified for electrodes in the STG to electrodes in the MTG and for electrodes in the STG to electrodes across the Sylvian fissure. An ANOVA was performed between groups for each distance, followed by post-hoc pairwise t-tests where applicable. The most convincing differences were in the low neural frequencies. The theta band observations are shown in Figure 8. For the theta frequency band at near distances, the STG-STG electrodes were more highly correlated than the STG-MTG electrodes and the STG-IFG (suprasylvian) electrodes. At distances of 5.65mm (for diagonally adjacent electrodes) and 4 mm, the STG-STG electrode correlations differ from STG-IFG correlations but do not differ significantly from the STG-MTG electrodes. This pattern is also seen for the alpha band. The pattern of significance suggests that within-gyrus correlations are highest, followed by within-lobe correlations, and finally across-lobe correlations on gyri. The pattern was not statistically significant for the beta to high gamma band. We surmise that this is due to the already-low correlations that are observed at the shortest observable distance of 4mm in these bands. We postulate that if the density of the grid were high enough, the same pattern would be observed in higher frequency bands as in the theta band; within-gyrus correlations are highest, followed by within-lobe correlations, and finally across-sulcus correlations.

**4. Discussion**

This study was done to empirically define the spatial spread function of ECoG signals towards

understanding the relationship of neural frequency with spatial spread of activity across electrodes. We quantitatively defined the relationship of neural signal correlation and spatial distance. We further quantified how frequency band components affect this relationship, as higher frequencies have higher spatial resolution than low frequencies. We compared the spatial spread function across patients and across functional gyri, and noted consistency in the spatial fall off across patients and across functionally distinct areas. We then examined the effect of gyral and sulcal structural anatomy on spatial correlations.

There are three major contributions to the observed positive spatial correlations, not including artifact or a common reference. First, there are correlations that are due simply to the physical properties of the measured electric field; this is referred to as volume conduction. The magnitude of electric fields decrease as a function of one over distance squared(Cybulski et al., 2014). Second, there are functional correlations in neural networks due to synaptic connectivity. These functional correlations could appear in regions far away from each other because networks are not constrained to neighboring areas. Third, there are correlations due to the properties of the underlying neurophysiological generators of electric signals. While the neural origins of the various canonical frequency bands are still a topic of debate, one theory is that low frequency signals are due to the spatial summation of synchronous dendritic inputs and that high frequency signals are the fields produced by spiking sub-populations and fast ionic and synaptic currents(Edwards et al., 2009, 2010; Lempka et al., 2011; Pesaran, 2009). If this is the case, low frequency correlations are more widespread than high frequency correlations because their generators act as a synchronous unit over a larger area than a high frequency spiking subpopulation. All three major categories of correlation are presumably represented in the dataset that we have analyzed in this paper.

To date, the closest study to the one presented here was a spatial correlation analysis of ECoG

signals across different electrode types in various places on the human cortex(Kellis et al., 2015). This was done using small microwire arrays in addition to large clinical arrays with 1cm spacing. The findings in this paper suggest similar patterns in spatial correlation fall off with distance for both tested arrays, for raw data. However, the reported spatial correlation fall offs are shallower than we observe. This is probably due to recording while the patient was not engaged in a task to specifically elicit activity in the recorded area. In our own analysis of correlations during rest versus activity, we observed a similar shallow fall off curve during rest. Interestingly, high-frequency modulation, which is believed to represent the activity of spatially localized neural processes, shows a greater change in correlation for rest versus task conditions than low frequency data. This is consistent with the idea that spatially discrete high frequency generators are recruited for a task, while low frequency generators maintain a brain state or modulate attention(Donner & Siegel, 2011; Engel & Fries, 2010). Importantly, our finding of stronger falloff of correlations during activity suggests that higher electrode densities may add specificity to observed task-related signals. Since distinct patterns of evoked activity may be observed even at small distances, increased spatial resolution may improve decoding of task-related output. Determining the optimal spacing between electrodes would allow us to determine at what spatial scale neural signals are redundant for a given task.

It would seem that the optimal spacing of electrodes would simply be to use the smallest inter-electrode distance possible that avoids shunting. However, there are other factors to consider. First, as density increases, electrode size necessarily decreases to make space and indeed to avoid electrical shunting. Smaller electrodes may not be ideal for electrocorticography recordings because they measure integrated activity of a smaller body of neural generators, and they potentially lose sensitivity to deeper cortical sources(Wodlinger, Degenhart, Collinger, Tyler-Kabara, & Wang, 2011). Furthermore, as electrodes become smaller their impedance increases, making the signal-to-noise ratio lower than similar electrodes of a larger scale.

Second, higher channel counts mean more wires, connectors, amplifiers, and data storage units. This is not trivial as channel counts increase into the thousands, though it may not be necessary if a more efficient use of materials can give a similar picture of the neural activity.

Considering the above as motivation, it is clear that determining the falloff of signal correlations over cortical distance has implications for the design of ECoG grids. Freeman et al. performed a study on the optimal spacing of electrodes in ECoG for signals recorded from the human STG and motor cortex(Freeman, Rogers, Holmes, & Silbergeld, 2000). The study was done with a linear microwire array, and it examined the spatial frequency of neural oscillations up to 50 Hz. The conclusion was that for these frequency bands, the smallest spatial frequency observed above the noise floor was one that corresponds to 2.5mm per cyclic spatial change. This correlates well with our shared variability observation for low frequency neural signals. Another more recent study(Slutzky et al., 2010), used modeling of neural dipoles to estimate the optimal spacing of surface electrodes for human cortex. The resulting recommendation for electrode spacing was 1.4mm correcting for Nyquist sampling, a measurement that again corresponds roughly to our observed and extrapolated correlations for low frequency neural data in the theta and alpha bands.

We have demonstrated the relationship between neural frequency and the spatial spread of signals at the cortical surface. Whether the application is during rest or active behavior will change the expected signal correlation over distance. The phase and amplitude observations have similar dependencies; however, phase correlations decrease more quickly with distance. This is of particular importance in the theta and alpha bands where phase is a common signal of interest.

Although this study included areas that were both sensorimotor and higher-order processing, correlations were computed for speech-related tasks in speech-related areas. Cortical encoding and tuning might be at different scales in other brain regions or even for other types of stimuli. A potential limitation of the fitting approach is that it leans toward the average of many data points, and therefore the resulting fit can over- or underestimate the activity spread from any one specific point. The results are an estimated fit averaged over several patients; as such, the cortical resolution suggested by these results should be interpreted as an average, not an absolute minimum. By the same token, taking the interquartile range leaves out the most highly correlated electrodes at each distance and can therefore be considered a conservative measure of shared signal.

Furthermore, our results provide novel information about the spatial spread of local field potential signals at the cortical surface. With ECoG grids of sufficient density and area, analysis of cortical activity can better describe the dynamics and functional connectivity of the cortex. Future studies can reveal if there are truly separable functional areas that respond to similar stimuli. The identification of functional areas corresponding to frequency of neural signal can shed light onto the origin of neural oscillations of various frequencies, most of which are not currently well understood.

**5. Conclusions**

The optimal spacing of ECoG electrodes depends heavily on the neural frequency band. The shape of the curve that defines this relationship is consistent across patients, but differs depending on which frequency band is represented and on which feature, amplitude or phase, is being represented. The dependence of this correlation falloff function on anatomical region is minimal, but falloff is stronger during speech-related tasks compared to rest. Correlations within functionally defined gyri are higher than those across sulci for low frequency oscillations.

**Acknowledgments**

The authors would like to thank M. Leonard, D. Moses, C. Tang, M. Sjerps, M. Baud, B. Dichter, D. Conant, G. Anumanchipalli, L. Frank, C. Schreiner, D. Lowenstein, and M. Maharbiz for helpful discussion on this work. This work was supported by grants from the NIH and the National Institute on Deafness and Other Communication Disorders (R01 DC012379 04, to EFC, and a Ruth L. Kirschstein Postdoctoral NRSA F32DC014192-01, to LSH), DARPA SUBNETS W911NF-14-2-0043, the William K. Bowes, Jr. Foundation, the Shurl and Kay Curci Foundation, and the McKnight Foundation.

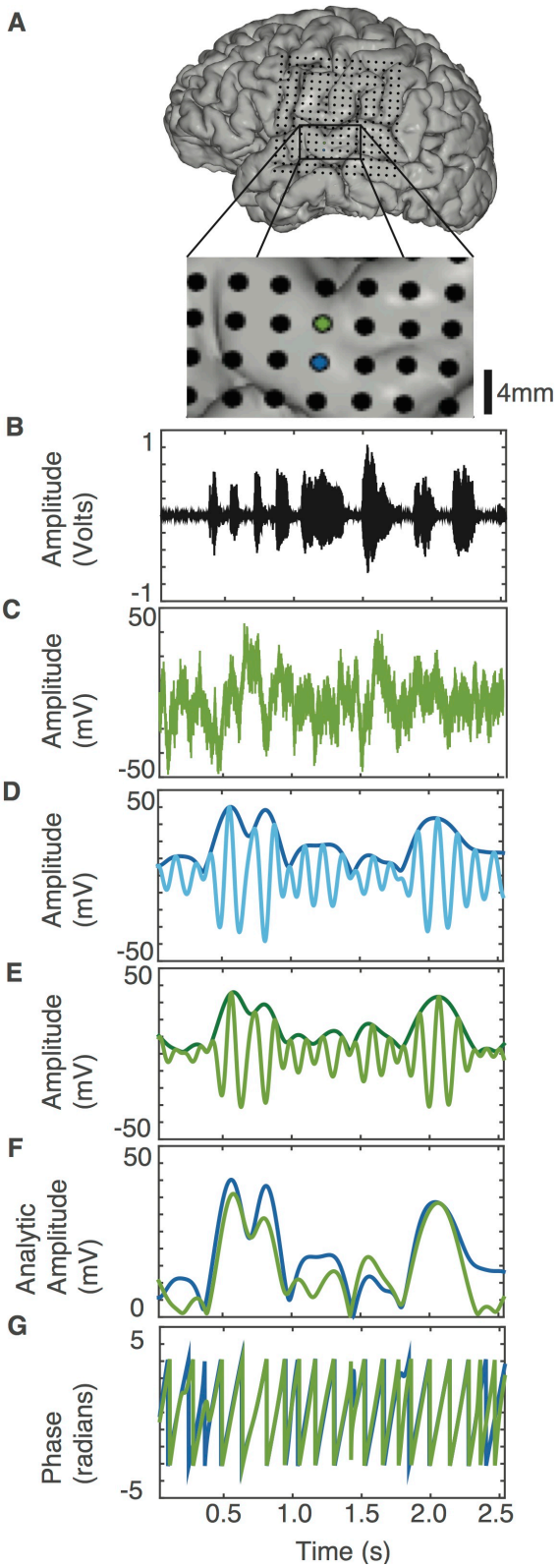


**Figure 1** Comparing ECoG signals from adjacent electrodes. (A) MRI reconstruction with CT co-registered electrode positions. (Inset) Two adjacent electrodes are spaced 4mm apart on the STG (green and blue). (B) Sound waveform of example sentence presented aurally. (C) Raw ECoG signal from green electrode (after notch filtering and common average referencing). (D-E) Time-locked neural signal from the blue (D) and the green (E) electrodes in the theta range. Light color shaded lines are bandpassed signal in the theta range, while dark colored lines are the analytic amplitude of the signal. (F) Analytic amplitudes are overlaid, and show high correlation (R=0.83, over approximately 5 minutes of data) (G) Phase traces for the same electrodes show high correlation (R=0.65, also over approximately 5 minutes of data).

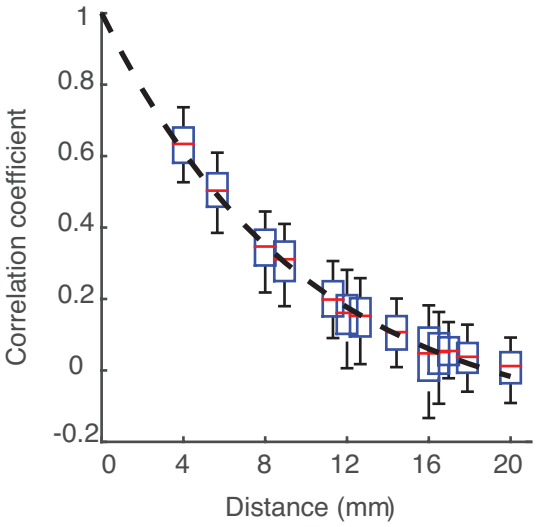


**Figure 2** Raw signal correlation decreases with distance. The falloff of correlation coefficient for pairs of neural signals as distance between electrode pairs increases. Blue outline represents the interquartile range of data. Red lines are the median of each plot. Black whisker lines represent the upper and lower quartiles of data. Black dashed line shows the exponential fit, chosen as such because it has the highest $R^2$ value of the functions that attempted to fit the data. There are no observations below 4mm, the closest spacing of electrodes.

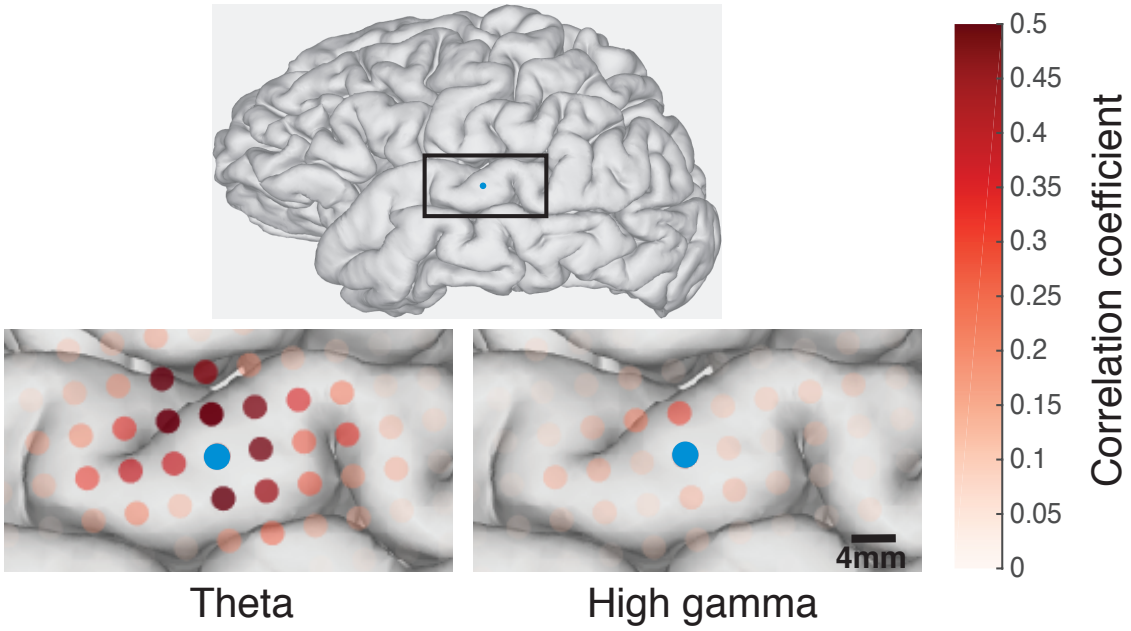


**Figure 3** Comparison of ECoG spatial spread for low and high spectral frequency bands. The part of the brain that is represented in the insets is shown in the boxed portion of the full brain above. In the inset to the left, correlations in analytic amplitude for the theta band are shown for one electrode. The same electrode is shown at right, along with correlations in the analytic amplitude of the high gamma frequency band. The theta band (left) shows higher correlations over a larger area than the high gamma band (right). The electrode to which all pairwise correlations are made is shown in blue for each.

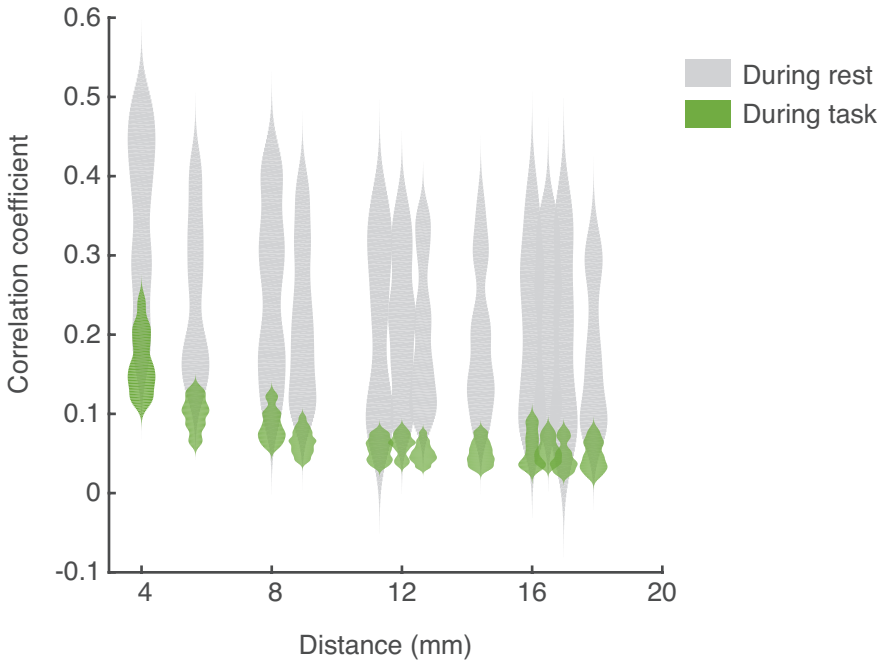


**Figure 4** Distributions of high gamma correlations for rest versus activity. Correlations decrease markedly in the high gamma frequency when the subject performs a task. Distributions at each distance are shown for the high gamma analytic amplitude activity for active electrodes in STG of one patient during a listening task. The gray plots show the distributed values of correlations between electrodes at each distance during rest, while the green plots show this distribution during the task. At each distance, the same number of data points are used to create the distributions in gray and green.

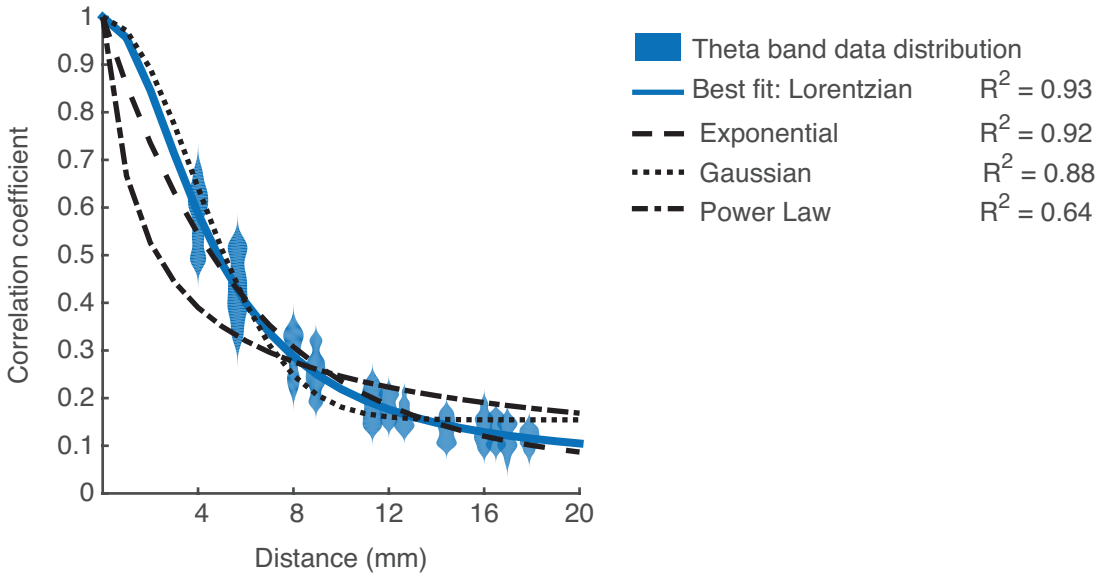


**Figure 5** Best fit functions approximate representative data (theta band analytic amplitude) for a single subject. A distribution plot of pairwise correlations at each distance are shown in blue. The best fit line for this component is a Lorentzian fit, shown by the line in blue. The Lorentzian form is followed closely in goodness-of-fit by the exponential form, shown by a dashed line. The goodness-of-fit further decreases for the Gaussian fit, and finally for the Power Law.

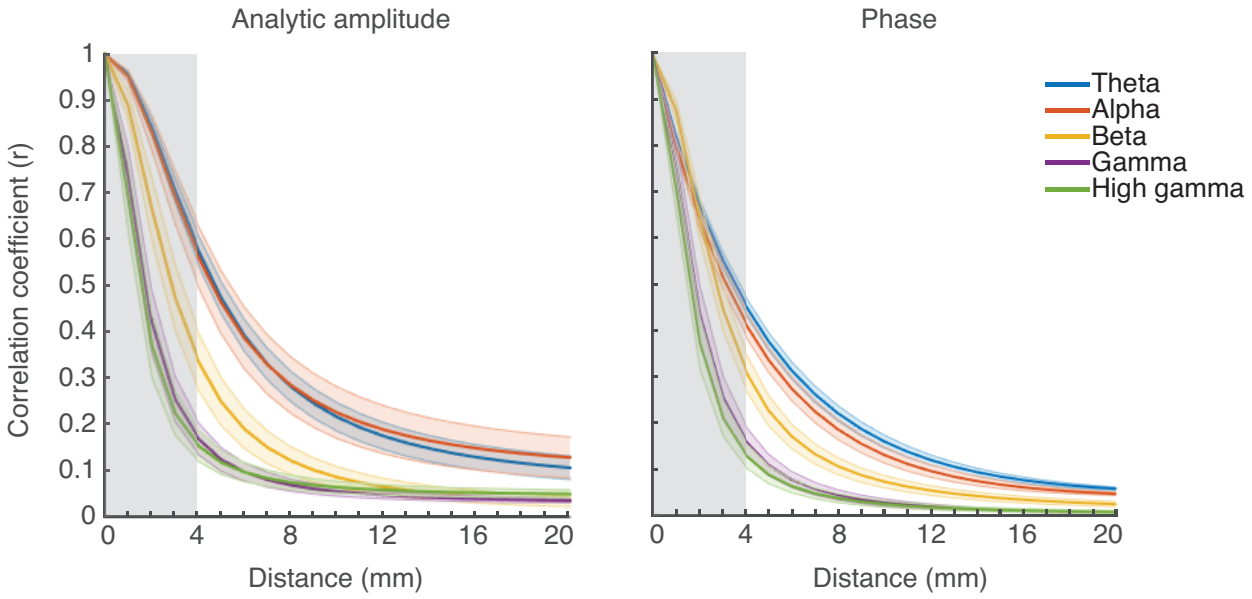


**Figure 6** Electrode pair correlations decrease predictably as a function of distance. A curve-fitting algorithm was used to fit four equations to the data. The fit with the highest R-squared value was chosen to represent the frequency band. Fit lines become steeper with increasing neural frequency for all patients, indicating a sharper falloff of shared variability for high frequency bands with distance. The result is averaged over five patients for active electrode pairs over the STG. Dark lines indicate the mean fit across patients; lighter background fill indicates standard error across patients. The gray shaded region is the region of the fit in which there were no neighboring electrode pairs below 4mm.

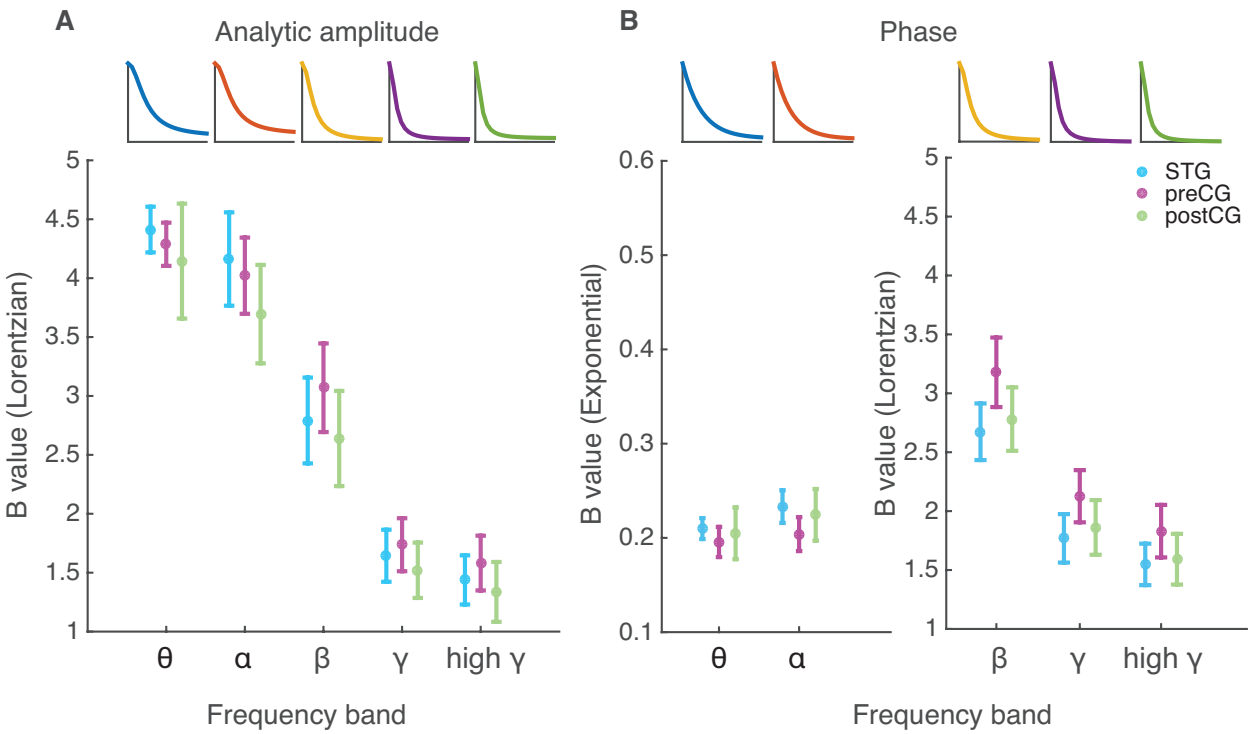


**Figure 7** The steepness of correlation falloff values are conserved across patients and cortical regions, but differ by frequency band. (A) The Lorentzian equation (see Methods, equation 2) is the equation of best fit to represent falloff of correlation with distance for all frequency bands. The B value is representative of the steepness of the curve. The mean and standard error of the B value across patients for each cortical area is represented with a center point and error bars at each frequency band. The error bars and points are color coded by cortical area. A representative curve is shown above for each frequency band to give an idea of the curve that is constructed with the average B value. (B) The exponential equation (see Methods, equation 1) is the equation of best fit to represent falloff of correlation with distance for theta and alpha frequency bands, while the Lorentzian fit best describes falloff of correlation with frequency for beta, gamma, and high gamma bands. The B value is representative of the steepness of the curve. The mean and standard error of the B value across patients for each cortical area is represented with a center point and error bars at each frequency band. The error bars and points are color coded by cortical area. A representative curve is shown above for each frequency band to give an idea of the curve that is constructed with the average B value.

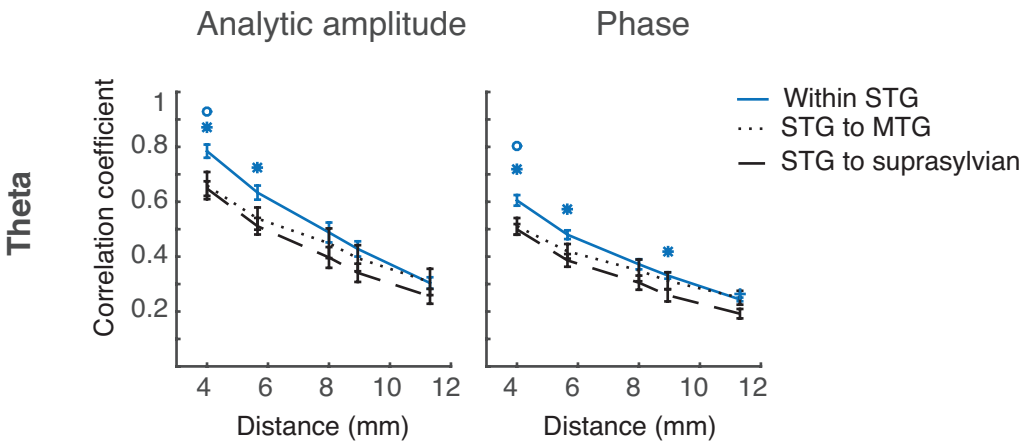


**Figure 8** Within gyrus, across sulcus, and across fissure correlation patterns for the theta band. Correlations within a gyrus trend higher than correlations across a sulcus or the Sylvian fissure. Mean and standard error of correlations over patients are plotted for electrodes within the STG (blue solid line), STG to MTG (dotted line), and STG to IFG (dashed line). This effect is more pronounced for amplitude correlations than phase correlations. Statistical significance, determined with an ANOVA followed by paired t-tests at each distance, is denoted by markers above each distance. An asterisk denotes a significance of $p<0.05$ between groups 'Within STG' and 'STG to suprasylvian.' A circle denotes significance of $p<0.05$ between groups 'Within STG' and 'STG to MTG.'

**References**


Blakely, T., Miller, K. J., Rao, R. P. N., Holmes, M. D., & Ojemann, J. G. (2008). Localization and classification of phonemes using high spatial resolution electrocorticography (ECoG) grids. *Conference Proceedings : ... Annual International Conference of the IEEE Engineering in Medicine and Biology Society. IEEE Engineering in Medicine and Biology Society. Conference*, *2008*, 4964–4967. doi:10.1109/IEMBS.2008.4650328

Bouchard, K. E., Mesgarani, N., Johnson, K., & Chang, E. F. (2013). Functional organization of human sensorimotor cortex for speech articulation. *Nature*, *495*, 327–32. doi:10.1038/nature11911

Breshears, J. D., Gaona, C. M., Roland, J. L., Sharma, M., Anderson, N. R., Bundy, D. T., … Leuthardt, E. C. (2011). Decoding motor signals from the pediatric cortex: implications for brain-computer interfaces in children. *Pediatrics*, *128*(1), e160–e168. doi:10.1542/peds.2010-1519

Bruns, A., Eckhorn, R., Jokeit, H., & Ebner, A. (2000). Amplitude envelope correlation detects coupling among incoherent brain signals. *Neuroreport*, *11*(7), 1509–1514. doi:10.1097/00001756-200005150-00028

Buckner, R. L., & Vincent, J. L. (2007). Unrest at rest: Default activity and spontaneous network correlations. *NeuroImage*, *37*(4), 1091–1096. doi:10.1016/j.neuroimage.2007.01.010

Buzsaki, G., & Draguhn, A. (2004). Neuronal oscillations in cortical networks. *Science*, *304*, 1926–1929. Retrieved from PM:15218136

Cohen, M. R., & Kohn, A. (2011). Measuring and interpreting neuronal correlations. *Nature Neuroscience*, *14*(7), 811–819. doi:10.1038/nn.2842

Crone, N., Boatman, D., Gordon, B., & Hao, L. (2001). Induced electrocorticographic gamma activity during auditory perception. *Clinical Neurophysiology*. Retrieved from

http://www.ncbi.nlm.nih.gov/entrez/query.fcgi?db=pubmed&cmd=Retrieve&dopt=AbstractPlus&list_uids=15166876286328992102related:ZnHv9p-Re9IJ\nhttp://linkinghub.elsevier.com/retrieve/pii/S1388245700005459

Crone, N. E., Korzeniewska, A., & Franaszczuk, P. J. (2011). Cortical gamma responses: Searching high and low. *International Journal of Psychophysiology*. doi:10.1016/j.ijpsycho.2010.10.013

Cybulski, T. R., Glaser, J. I., Marblestone, A. H., Zamft, B. M., Boyden, E. S., Church, G. M., & Kording, K. P. (2014). *Spatial Information in Large-Scale Neural Recordings*. *bioRxiv*. doi:10.1101/002923

Donner, T. H., & Siegel, M. (2011). A framework for local cortical oscillation patterns. *Trends in Cognitive Sciences*. doi:10.1016/j.tics.2011.03.007

Edwards, E., Nagarajan, S. S., Dalal, S. S., Canolty, R. T., Kirsch, H. E., Barbaro, N. M., & Knight, R. T. (2010). Spatiotemporal imaging of cortical activation during verb generation and picture naming. *NeuroImage*, *50*(1), 291–301. doi:10.1016/j.neuroimage.2009.12.035

Edwards, E., Soltani, M., Kim, W., Dalal, S. S., Nagarajan, S. S., Berger, M. S., & Knight, R. T. (2009). Comparison of time-frequency responses and the event-related potential to auditory speech stimuli in human cortex. *Journal of Neurophysiology*, *102*(1), 377–386. doi:10.1152/jn.90954.2008

Elston, G. N. (2003). Cortex, Cognition and the Cell: New Insights into the Pyramidal Neuron and Prefrontal Function. *Cerebral Cortex*. doi:10.1093/cercor/bhg093

Engel, A. K., & Fries, P. (2010). Beta-band oscillations-signalling the status quo? *Current Opinion in Neurobiology*. doi:10.1016/j.conb.2010.02.015

Flinker, A., Chang, E. F., Barbaro, N. M., Berger, M. S., & Knight, R. T. (2011). Sub-centimeter language organization in the human temporal lobe. *Brain and Language*, *117*, 103–109.

doi:10.1016/j.bandl.2010.09.009

Freeman, W. J., Rogers, L. J., Holmes, M. D., & Silbergeld, D. L. (2000). Spatial spectral analysis of human electrocorticograms including the alpha and gamma bands. *Journal of Neuroscience Methods*, *95*, 111–121. doi:10.1016/S0165-0270(99)00160-0

Fries, P., Nikolić, D., & Singer, W. (2007). The gamma cycle. *Trends in Neurosciences*. doi:10.1016/j.tins.2007.05.005

Fukushima, M., Saunders, R. C., Leopold, D. A., Mishkin, M., & Averbeck, B. B. (2012). Spontaneous High-Gamma Band Activity Reflects Functional Organization of Auditory Cortex in the Awake Macaque. *Neuron*, *74*(5), 899–910. doi:10.1016/j.neuron.2012.04.014

Garofolo, J. (1993). TIMIT Acoustic-Phonetic Continuous Speech Corpus LDC93S1.

Kajikawa, Y., & Schroeder, C. E. (2011). How local is the local field potential? *Neuron*, *72*, 847–858. doi:10.1016/j.neuron.2011.09.029

Katzner, S., Nauhaus, I., Benucci, A., Bonin, V., Ringach, D. L., & Carandini, M. (2009). Local Origin of Field Potentials in Visual Cortex. *Neuron*, *61*, 35–41. doi:10.1016/j.neuron.2008.11.016

Kellis, S., Miller, K., Thomson, K., Brown, R., House, P., & Greger, B. (2010). Decoding spoken words using local field potentials recorded from the cortical surface. *Journal of Neural Engineering*, *7*, 056007. doi:10.1088/1741-2560/7/5/056007

Kellis, S., Sorensen, L., Darvas, F., Sayres, C., O'Neill, K., Brown, R., … Greger, B. (2015). Multi-scale analysis of neural activity in humans: implications for micro-scale electrocorticography. *Clinical Neurophysiology*, 1–11. doi:10.1016/j.clinph.2015.06.002

Kent, A. R., & Grill, W. M. (2014). Analysis of deep brain stimulation electrode characteristics for neural recording. *Journal of Neural Engineering*, *11*, 046010. doi:10.1088/1741-2560/11/4/046010

Khodagholy, D., Gelinas, J. N., Thesen, T., Doyle, W., Devinsky, O., Malliaras, G. G., & Buzsaki, G. (2015). NeuroGrid: recording action potentials from the surface of the brain. *Nat Neurosci*, *18*(2), 310–315. Retrieved from http://dx.doi.org/10.1038/nn.3905

Lachaux, J.-P., Axmacher, N., Mormann, F., Halgren, E., & Crone, N. E. (2012). High-frequency neural activity and human cognition: Past, present and possible future of intracranial EEG research. *Progress in Neurobiology*. doi:10.1016/j.pneurobio.2012.06.008

Lempka, S. F., Johnson, M. D., Moffitt, M. A., Otto, K. J., Kipke, D. R., & McIntyre, C. C. (2011). Theoretical analysis of intracortical microelectrode recordings. *Journal of Neural Engineering*, *8*, 045006. doi:10.1088/1741-2560/8/4/045006

Leski, S., Lindén, H., Tetzlaff, T., Pettersen, K. H., & Einevoll, G. T. (2013). Frequency Dependence of Signal Power and Spatial Reach of the Local Field Potential. *PLoS Computational Biology*, *9*(7). doi:10.1371/journal.pcbi.1003137

Leuthardt, E. C., Freudenberg, Z., Bundy, D., & Roland, J. Microscale recording from human motor cortex: implications for minimally invasive electrocorticographic brain-computer interfaces., 27 Neurosurgical focus E10 (2009). doi:10.3171/2009.4.FOCUS0980

Miller, K. J., Leuthardt, E. C., Schalk, G., Rao, R. P. N., Anderson, N. R., Moran, D. W., … Ojemann, J. G. (2007). Spectral changes in cortical surface potentials during motor movement. *The Journal of Neuroscience : The Official Journal of the Society for Neuroscience*, *27*(9), 2424–2432. doi:10.1523/JNEUROSCI.3886-06.2007

Pesaran, B. (2009). Uncovering the Mysterious Origins of Local Field Potentials. *Neuron*. doi:10.1016/j.neuron.2008.12.019

Pesaran, B. (2010). Neural correlations, decisions, and actions. *Current Opinion in Neurobiology*. doi:10.1016/j.conb.2010.03.003

Ray, S., Crone, N. E., Niebur, E., Franaszczuk, P. J., & Hsiao, S. S. (2008). Neural correlates of

high-gamma oscillations (60-200 Hz) in macaque local field potentials and their potential implications in electrocorticography. *The Journal of Neuroscience : The Official Journal of the Society for Neuroscience*, *28*, 11526–11536. doi:10.1523/JNEUROSCI.2848-08.2008

Slutzky, M. W., Jordan, L. R., Krieg, T., Chen, M., Mogul, D. J., & Miller, L. E. (2010). Optimal spacing of surface electrode arrays for brain-machine interface applications. *Journal of Neural Engineering*, *7*, 26004. doi:10.1088/1741-2560/7/2/026004

Viventi, J., Kim, D.-H., Vigeland, L., Frechette, E. S., Blanco, J. A., Kim, Y.-S., … Litt, B. (2011). Flexible, foldable, actively multiplexed, high-density electrode array for mapping brain activity in vivo. *Nature Neuroscience*. doi:10.1038/nn.2973

Wang, W., Degenhart, A. D., Collinger, J. L., Vinjamuri, R., Sudre, G. P., Adelson, P. D., … Weber, D. J. (2009). Human motor cortical activity recorded with Micro-ECoG electrodes, during individual finger movements. *Conference Proceedings : ... Annual International Conference of the IEEE Engineering in Medicine and Biology Society. IEEE Engineering in Medicine and Biology Society. Annual Conference*, *2009*, 586–9. doi:10.1109/IEMBS.2009.5333704

Wodlinger, B., Degenhart, A. D., Collinger, J. L., Tyler-Kabara, E. C., & Wang, W. (2011). The impact of electrode characteristics on electrocorticography (ECoG). In *Proceedings of the Annual International Conference of the IEEE Engineering in Medicine and Biology Society, EMBS* (pp. 3083–3086). doi:10.1109/IEMBS.2011.6090842

Womelsdorf, T., & Fries, P. (2007). The role of neuronal synchronization in selective attention. *Current Opinion in Neurobiology*. doi:10.1016/j.conb.2007.02.002

Wrench, A. (1999). The MOCHA-TIMIT articulatory database.

Xing, D., Yeh, C.-I., & Shapley, R. M. (2009). Spatial spread of the local field potential and its laminar variation in visual cortex. *The Journal of Neuroscience : The Official Journal of the*

*Society for Neuroscience*, *29*, 11540–11549. doi:10.1523/JNEUROSCI.2573-09.2009

# Thin-film, high-density micro-electrocorticographic decoding of a human cortical gyrus

Leah Muller[1], Sarah Felix[2], *Member, IEEE,* Kedar G. Shah[2], Kye Lee, Satinderpall Pannu[2], *Member, IEEE,* and Edward F. Chang[1]

***Abstract*— High-density electrocorticography (ECoG) arrays are promising interfaces for high-resolution neural recording from the cortical surface. Commercial options for high-density arrays are limited, and historically tradeoffs must be made between spatial coverage and electrode density. However, thin-film technology is a promising alternative for generating electrode arrays capable of large area coverage and high channel count, with resolution on the order of cortical columns in the functional surface unit of a human gyrus. Here, we evaluate the sensing performance of a high-density thin-film 128-electrode array designed specifically for recording the distributed neural activity of a single human cortical gyrus. We found robust field potential responses throughout the superior temporal gyrus evoked by speech sounds, and clear phonetic feature selectivity at the resolution of 2 mm inter-electrode distance. Decoding accuracy improved with increasing density of electrodes over all three patients tested. Thin-film ECoG has significant potential for high-density neural interface applications at the scale of a human gyrus.**

***Index terms*— electrocorticography, micro-ECoG, brain machine interface, neural device design, spatial resolution, neural decoding, thin film, high density**

## I. Introduction

Electrocorticography (ECoG) is a method of recording electrical neural signals from the cortical surface. Traditionally, ECoG has been used to localize the seizure focus in patients with refractory epilepsy for

[1]L. Muller and E. Chang are with University of California, San Francisco, 675 Nelson Rising Lane, Room 511, San Francisco, CA 94158, USA. (e-mail: Edward.Chang@ ucsf.edu).

[2]S. Felix, K. Shah, K. Lee, and S. Pannu are with Lawrence Livermore National Laboratory, 7000 East Avenue, Livermore, CA 94550.

This work was supported by grants from the NIH and the National Institute on Deafness and Other Communication Disorders (R01 DC012379 04, to EFC, DARPA SUBNETS W911NF-14-2-0043, and a University of California Office of the President Research Grant. Work was performed under the auspices of the U.S. Department of Energy by the Lawrence Livermore National Laboratory under contract number DE-AC52-07NA27344.

surgical planning. Most currently available clinical electrode arrays have one centimeter center-to-center electrode spacing. There are many emerging applications, such as brain-computer interfaces (BCIs), in which sensing resolution on a much finer scale is required. In particular, there is a need for new neural interface devices that are capable of recording neural activity on the order of cortical columns, an important spatial unit of cortical organization.

Micro-electrocorticography (μECoG) refers to ultra high-density recordings with spacing on the order of microns to millimeters. An important feature of μECoG is the potential to record high-density neural activity safely, while also conforming to a specific anatomic region-of-interest. The technology used to make these multi-electrode arrays must necessarily be different than that for hand-made, commercially available electrode arrays.

We have utilized thin-film MEMS technology to fabricate a new μECoG multi-electrode array for human application. The array was designed to leverage the safety and low impedance properties of disk-type electrodes for the cortical surface, while also increasing density. The technological platform is a flexible one, so the same manufacturing technique can be applied to a variety of array configurations of surface area, electrode size, electrode shape, array pattern, electrode number, and density. Here we show high-resolution recording and discrimination of speech sounds using the thin-film array in human subjects as a demonstration of their potential for neural interface applications.

## II. Experimental Methods

### *A. μECoG design and fabrication*

The μECoG array consists of 128 electrodes (8x16), 1.2 mm in diameter with a center-to-center spacing of 2mm, designed specifically to span a human cortical gyrus. The thin film arrays were designed and fabricated in a similar manner as detailed in [1]. Polyimide layers provided insulation and structure between each metal layer, making the array a total thickness of approximately 20μm. Thin-film Ti/Au/Ti was sputter-deposited and patterned using contact lithography and wet etching to form conductive traces. Vias were etched in the polyimide using oxygen plasma to provide electrical contact between the electrode metal layer and the trace metal. The electrode metal layer was added by sputter depositing 250nm of Pt over a Ti adhesion layer and patterning the metal using contact lithography and reactive-ion etching.

Finally, oxygen plasma was used to etch openings on top of electrodes and connector pads. Each μECoG array was wire-bonded to a silicon interconnect board that was subsequently potted in medical grade epoxy. Electrode impedances at 1kHz were in the range of 800-900 kΩ.

*B. Experimental setup*

Experimental procedures were approved by the Committee for Human Research at the University of California, San Francisco and the Lawrence Livermore National Laboratory Institutional Review Board. All participants provided written informed consent. Three patients undergoing an awake craniotomy with language mapping prior to resection of epileptic foci volunteered to participate in this research study. In all three patients, the human auditory speech cortex, superior temporal gyrus (STG), was exposed as part of the clinical procedure. The sterilized thin-film μECoG device was placed on the STG, where cortical responses can be evoked in response to speech sounds[2], [3]. A needle electrode in the scalp served as the reference electrode and ground. The subjects listened to 51 pseudo-randomized consonant-vowel (CV) syllables played through free-field speakers. The inter-stimulus interval was 2.25 seconds with a jitter of up to 250ms. Presentation of experimental stimuli was synchronized to neural recordings.

*C. Recording and data processing*

Signals were acquired at a sampling rate of 3051.8 Hz and were amplified and digitized using a Tucker-Davis Technologies neural recording system. Manual artifact and channel rejection was performed, followed by common average referencing (CAR) [4]. The CAR consists of the mean across 64-channel banks of non-rejected electrodes that are spatially arranged in four rows that span 3.5cm x 1.2cm. The CAR approximates the activity contributed by the original reference, so subtracting the CAR from each channel largely removes contributions of the original reference electrode and electrical artifacts that are often present in groups of 64 channels due to shared connectors and cabling (see Crone et al. 2001 for a discussion of CAR in ECoG recordings).

## III. Analytical methods

### A. Signal processing

The signal from each electrode channel was filtered into 56 frequency bands using an FFT followed by a Hilbert transform with logarithmically increasing center frequencies (range of CF = 4.07 Hz – 944.83 Hz). The analytic amplitude, also known as the envelope, was calculated for each [5]. The filtered frequencies were then averaged over high gamma (70 – 150 Hz) bands. The natural log of this signal was then z-scored with respect to rest (no-task) epochs within the same recording.

Electrodes were chosen for analysis using a bootstrap t-test to find electrodes that responded significantly to speech over silence. The threshold p-value for inclusion was 0.001 over 10,000 bootstrap iterations.

### B. Decoding analysis

To test decoding performance, the z-scored log of the high gamma analytic amplitude was used as the signal for significantly modulated electrodes (defined above). Classification was done using Linear Discriminant Analysis (LDA) and trained on four phonetic feature categories of sounds for which the STG neurons are known to express selectivity [2]: ‘fricatives’, ’nasals’, ’glides’, and ‘stops.’ A leave-one-out cross validation was employed to generate performance metrics. High gamma responses were taken for ten evenly spaced time points 200ms to 300ms after the onset of the syllable and associated with a phonetic category. The average of the correct predicted categories for each ten-time-point representation of the CV was used as the percent correct for each CV syllable prediction. These were averaged together to get a final metric of ‘percent correct.’

The electrode array was spatially subsampled at 4mm and 8mm inter-electrode spacing for all possible subsample variations. The variation in performance between spatial shifts of the same decimation factor was small, and results are reported as an average over all possible spatial subsamples for 4 and 8mm.

## IV. Results

The goal of our study was to functionally validate the sensing performance of a novel thin-film μECoG device for human recordings. We verified that evoked responses can be successfully recorded in the

frequency range of interest for neural recordings. We then compared decoding accuracy using all responsive electrodes and decimated subsets of those electrodes.

In contrast to commercially available high-density grids for surface recordings, the thin-film μECoG has not only large surface area but also high density. The surface area and density are highlighted in Fig. 1. The thin-film array covers approximately the width of a human gyrus. It is low profile and extremely flexible to be conformal to the brain's surface.

A schematic of the array on the surface of the STG is shown in Fig. 2. Fig. 2B shows a typical single-electrode response to an acoustic stimulus. Robust evoked neural responses are recorded across the array, as shown in Fig. 2C. Several electrodes did not record good responses, possibly due to placement over small cortical blood vessels or faulty electrodes.

Single electrodes show selectivity for phonetic features. An example is shown in Fig. 3A, where one electrode's mean responses to the four phonetic categories tested is plotted. This electrode is selective for stops. We wanted to determine if, for the same available surface area of the human STG, a higher density of electrodes increases decoding accuracy. Results of this analysis are shown in Fig. 4. With chance at 25%, we see that neural activity for all center-to-center spacings boosts predictive performs over chance. Beyond this observation, decoding performance increases as spatial density increases.

## V. Discussion

Our goal was to evaluate the human-based physiological recording properties of a high-density ECoG device fabricated using MEMS-based thin-film technology. Here we show that thin-film μECoG can record robust human cortical signals. We showed that there are differences in phoneme feature selectivity at single electrodes. Across all three patients, we see an improvement in decoding accuracy with increased spatial resolution in the same available area.

In the last decade, thin-film MEMS-based electrode arrays have proven their utility in animal ECoG studies [6]–[12]. The technology is appealing because the arrays are highly conformal to the brain's surface, and the fabrication platform allows for scalable, customizable designs. The micron-level precision enables the fabrication of extremely small electrodes and very dense center-to-center spacing. Some groups have capitalized on the flexibility of the thin-films, making arrays that can be bent to record within a

sulcus [7], [12]. A recent study used thin-film devices in humans intra-operatively to record spontaneous surface potentials [13]. However, to our knowledge, this represents the first validation of a thin-film array that demonstrates recording of functional evoked activity from human cortex. Additionally, our array highlights the advantages of maintaining broad spatial coverage while increasing number of electrodes within an anatomical area.

Our combination of large surface area and dense spacing of electrodes allows us to interrogate a functionally related area on a human gyrus at high resolution. Spatial resolution improvements are obviously meaningful, as increased density improves decoding performance. This could be due to boosting of the signal-to-noise ratio from pooled estimates of a signal over electrodes. Alternatively, it could mean that the brain actually represents information at the scale of 2mm or less, information that is not captured with low-density sampling. We have evidence that higher density improves decoding, and with even higher density we may see further decoding benefits.

## VI. Conclusions

We have concluded that the thin-film µECoG array is a viable technology for recording neural signals from the human cortical surface. This technology is a good alternative to commercially available high-density options, as the arrays are safe, conformal, and relatively low impedance. The thin-film arrays are capable of recording robust and discrete high gamma signals even at a spacing of 2mm center-to-center. Higher density recordings enhance neural decoding capability within single patients, and the limit to this improvement has not yet been reached.

## VII. Acknowledgments

The authors would like to thank M. Leonard, L. Hamilton, E. Edwards, D. Moses, C. Tang, M. Sjerps, B. Dichter, D. Conant, L. Frank, C. Schreiner, D. Lowenstein, and M. Maharbiz for helpful discussion on this work.

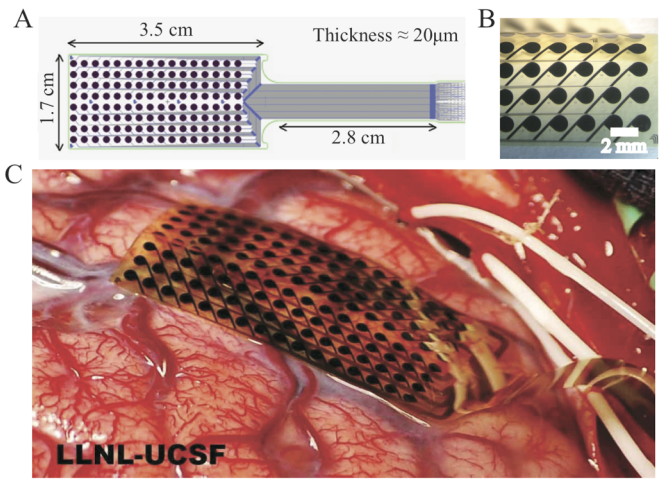


*Figure 1.* LLNL-UCSF thin-film array for human cortical recordings. (A) Schematic showing array layout. (B) Magnified view of thin-film µECoG array. Center-to-center spacing of electrodes is 2mm. Exposed electrode diameter is 1.2 mm. The array is thin and flexible, and the surface texture is smooth. Electrode positioning is precise to the order of microns. (C) Thin-film µECoG array on the surface of the human brain.

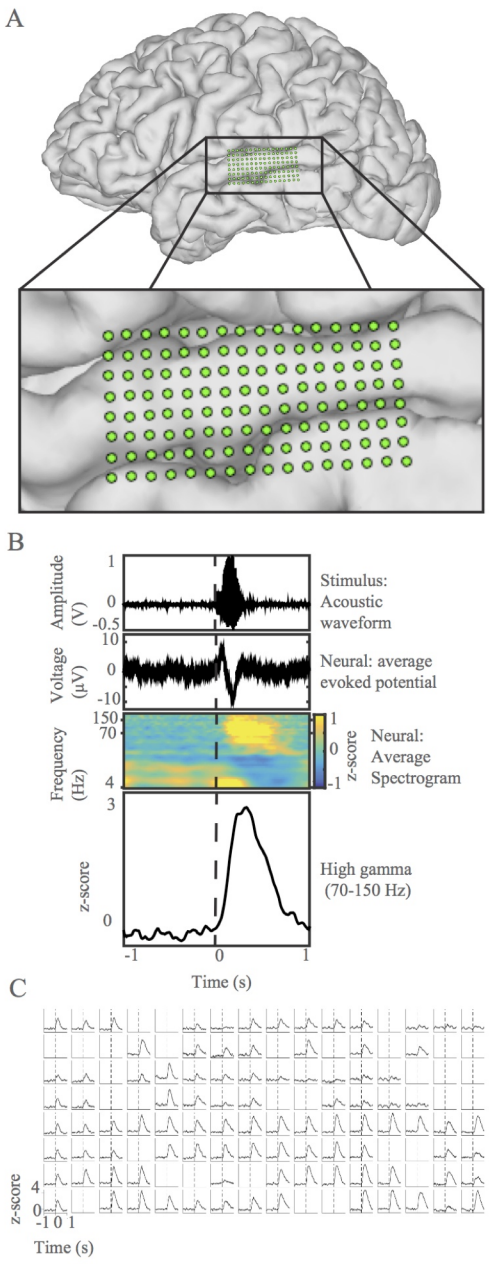


*Figure 2.* Thin-film array records robust evoked potentials. (A) MRI reconstruction of one subject's brain with μECoG array overlaid. Inset zooms in on μECoG on STG (B) Single electrode response to acoustic stimulus, time-locked to acoustic stimulus presentation. Dotted line marks stimulus onset. Top: Representative acoustic waveform of consonant-vowel stimulus. Second: Average raw evoked potential of neural signal. Third: Event-related cortical spectrogram. Each frequency band was individually z-scored on silence. Bright yellow areas show time points with relatively high activity in comparison to silence. Fourth: Evoked potential traces in time for z-scored high gamma band. (C) Robust high gamma responses are shown for each electrode site on the array. Each subplot represents the average high gamma response of the electrode at that location to the stimulus. Standard error is represented as a shaded area around each line and is very low. Dotted lines mark stimulus onset. Rejected channels are left blank.

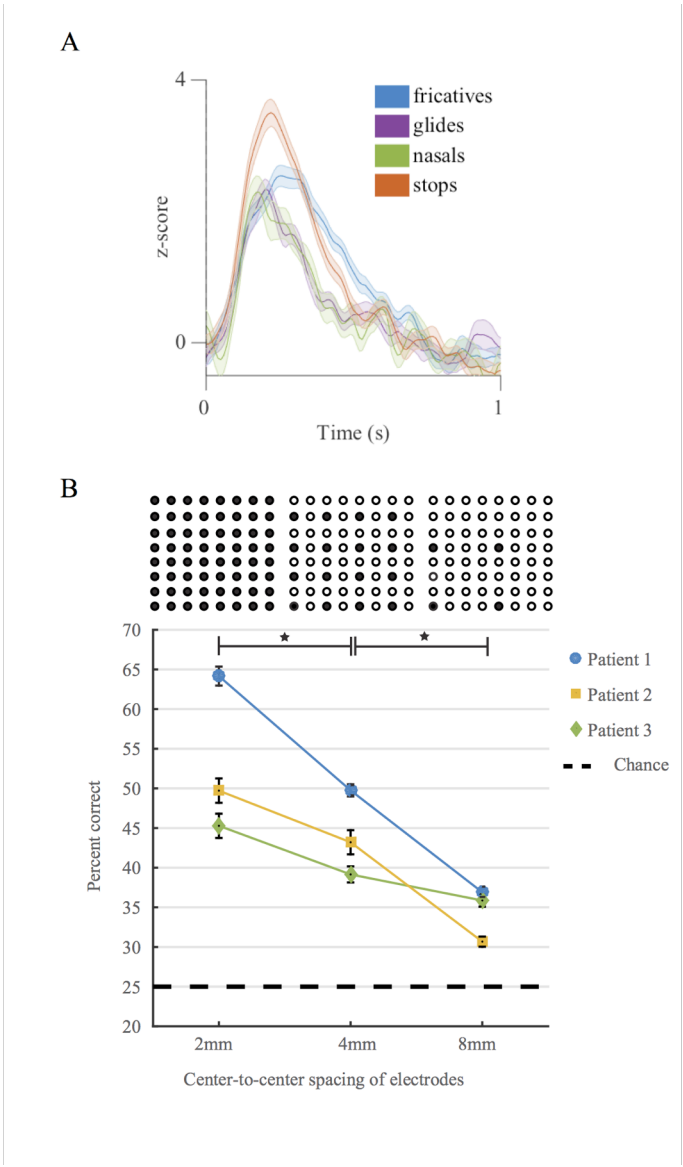


*Figure 3.* Single electrode selectivity and population decoding. A. High gamma phonetic feature selectivity for a representative electrode. (Average evoked potential - solid line; standard error of the mean - shaded). ERPs are color coded by phonetic category. B. Population decoding accuracy increases with higher density electrode sampling within the same surface area. Example electrodes included in each variation of the spacing designated on the x-axis are shown above the graph in agreement with the x-axis labels. Percent of correctly classified phonetic categories is presented as a function of electrode spacing. Chance performance is 25% and is plotted as a dotted line. Mean is plotted with error bars for percent correct at each density, subsampled from the same array. There is a significant increase in decoding accuracy as center-to-center spacing decreases. This is true for all three patients and is designated with a star at the top of the graph between the relevant center-to-center spacings.

## References


[1] A. Tooker, V. Tolosa, K. G. Shah, H. Sheth, S. Felix, T. Delima, and S. Pannu, “Optimization of multi-layer metal neural probe design,” in *Proceedings of the Annual International Conference of the IEEE Engineering in Medicine and Biology Society, EMBS*, 2012, pp. 5995–5998.

[2] N. Mesgarani, C. Cheung, K. Johnson, and E. F. Chang, “Phonetic feature encoding in human superior temporal gyrus.,” *Science*, vol. 343, no. 6174, pp. 1006–10, 2014.

[3] E. F. Chang, J. W. Rieger, K. Johnson, M. S. Berger, N. M. Barbaro, and R. T. Knight, “Emergence of Categorical Speech Representation in the Human Superior Temporal Gyrus,” *Nat. Neurosci.*, vol. 13, no. 11, pp. 1428–1432, 2010.

[4] N. Crone, D. Boatman, B. Gordon, and L. Hao, “Induced electrocorticographic gamma activity during auditory perception,” *Clinical Neurophysiology*. 2001.

[5] E. Edwards, M. Soltani, W. Kim, S. S. Dalal, S. S. Nagarajan, M. S. Berger, and R. T. Knight, “Comparison of time-frequency responses and the event-related potential to auditory speech stimuli in human cortex.,” *J. Neurophysiol.*, vol. 102, pp. 377–386, 2009.

[6] B. Rubehn, C. Bosman, R. Oostenveld, P. Fries, and T. Stieglitz, “A MEMS-based flexible multichannel ECoG-electrode array.,” *J. Neural Eng.*, vol. 6, p. 036003, 2009.

[7] T. Matsuo, K. Kawasaki, T. Osada, H. Sawahata, T. Suzuki, M. Shibata, N. Miyakawa, K. Nakahara, A. Iijima, N. Sato, K. Kawai, N. Saito, and I. Hasegawa, “Intrasulcal electrocorticography in macaque monkeys with minimally invasive neurosurgical protocols.,” *Front. Syst. Neurosci.*, vol. 5, p. 34, 2011.

[8] M. Fukushima, R. C. Saunders, M. Mullarkey, A. M. Doyle, M. Mishkin, and N. Fujii, “An electrocorticographic electrode array for simultaneous recording from medial, lateral, and intrasulcal surface of the cortex in macaque monkeys,” *J. Neurosci. Methods*, vol. 233, pp. 155–165, 2014.

[9] P. Ledochowitsch, R. J. Felus, R. R. Gibboni, A. Miyakawa, S. Bao, and M. M. Maharbiz, “Fabrication and testing of a large area, high density, parylene MEMS microECoG array,” *2011 IEEE 24th Int. Conf. Micro Electro Mech. Syst.*, pp. 1031–1034, 2011.

[10] P. Ledochowitsch, a. C. Koralek, D. Moses, J. M. Carmena, and M. M. Maharbiz, “Sub-mm functional decoupling of electrocortical signals through closed-loop BMI learning,” *Proc. Annu. Int. Conf. IEEE Eng. Med. Biol. Soc. EMBS*, pp. 5622–5625, 2013.

[11] S. Thongpang, T. J. Richner, S. K. Brodnick, a. Schendel, J. Kim, J. a. Wilson, J. Hippensteel, L. Krugner-Higby, D. Moran, a. S. Ahmed, D. Neimann, K. Sillay, and J. C. Williams, “A Micro-Electrocorticography Platform and Deployment Strategies for Chronic BCI Applications,” *Clin. EEG Neurosci.*, vol. 42, no. 4, pp. 259–265, 2011.

[12] J. Viventi, D.-H. Kim, L. Vigeland, E. S. Frechette, J. A. Blanco, Y.-S. Kim, A. E. Avrin, V. R. Tiruvadi, S.-W. Hwang, A. C. Vanleer, D. F. Wulsin, K. Davis, C. E. Gelber, L. Palmer, J. Van der Spiegel, J. Wu, J. Xiao, Y. Huang, D. Contreras, J. A. Rogers, and B. Litt, “Flexible, foldable, actively multiplexed, high-density electrode array for mapping brain activity in vivo,” *Nature Neuroscience*, vol. 14. pp. 1599–1605, 2011.

[13] D. Khodagholy, J. N. Gelinas, T. Thesen, W. Doyle, O. Devinsky, G. G. Malliaras, and G. Buzsaki, “NeuroGrid: recording

action potentials from the surface of the brain," *Nat Neurosci*, vol. 18, no. 2, pp. 310–315, Feb. 2015.

# Direct electrical stimulation evokes high gamma activity that predicts conscious somatosensory perception


## Authors

Leah Muller[1], John Rolston[1], Neal P. Fox[1], Robert Knowlton[2], Vikram Rao[2], and Edward F. Chang[1].

[1]Department of Neurosurgery, University of California, San Francisco, San Francisco, CA. [2]Department of Neurology, University of California, San Francisco, San Francisco, CA. Correspondence should be addressed to E.C. (Edward.Chang@ucsf.edu).



## Abstract

**Direct electrical stimulation (DES) is a clinical gold standard for human brain mapping, and readily evokes conscious percepts, yet the neurophysiological changes underlying these percepts are not well understood. To determine the neural correlates of DES, we stimulated the somatosensory cortex of ten human participants at stimulation frequency-amplitude combinations that both elicited and failed to elicit conscious percepts, meanwhile recording neural activity directly adjacent to and surrounding the stimulation site. We then compared the neural activity of perceived trials to that of unperceived trials. We found that stimulation evokes high gamma activation, and this neural activation correlates with conscious perception better than stimulation parameters alone. Our findings suggest that high gamma activity is a reliable biomarker for perception evoked by natural and electrical stimuli.**

Direct electrical stimulation (DES)—the direct application of electrical current to the cortical surface—has been used clinically since the early 1900's to map human functional anatomy.[1–5] DES mapping is routinely used to guide surgical decisions by identifying patient-specific brain regions critical for perceptual or cognitive functions such as sensation, motor control, and speech.[6–13] These inferences rely on the fundamental assumption that DES causes neural activity to change in a way that is consistent with that of natural stimuli. However, although recent work has provided strong evidence linking stimulation site and intensity to properties of a patient's subjective experience of naturally and artificially evoked percepts[14,15], the neural effects of DES remain unknown.[16,17] The present study represents the first systematic investigation of the neurophysiological effects of DES at clinically relevant levels.

Neural changes in response to DES have proven difficult to study, with most studies instead relying only on behavioral reports of overt percepts elicited by stimulation.[14,18–20] This focus away from electrophysiology stems in part from the technical challenges associated with simultaneous stimulation and recording of neural activity. First, saturation of amplifiers makes it impossible to recover neural signals during stimulation and for a short period after. Second, broad cortical coverage by many electrodes is necessary to determine the extent of the cortical surface affected by stimulation, and this is rarely achieved. Our experimental setup overcomes these technical obstacles by employing a high dynamic range amplifier for recording neural data from a high-density, broad-coverage electrocorticography (ECoG) array surrounding the site of stimulation.

With these technical advances, we sought to document the electrophysiological changes associated with DES-induced percepts. Prior ECoG studies of the somatosensory cortex have shown that high gamma neural activity increases in relation to sensory perception.[21] We therefore hypothesized that the artificial percepts induced by DES would share this underlying electrophysiological signature. Moreover, we hypothesized that high gamma activity was specifically related to the conscious perception of a stimulus and not just an artifact of electrically exciting tissue.

To assess the effects of DES on neural activity, we tested 10 patients who were undergoing clinical mapping prior to neurosurgical resection. We recorded before, during, and after electrical stimulation in somatosensory cortex using high-density ECoG grids surrounding and extending centimeters from the stimulation site. We defined the relationship between stimulation parameters of frequency and amplitude and the perceptual threshold. However, when examined on a trial-by-trial basis, we found in many cases in which above-threshold stimulation did not evoke a sensory percept. Analysis of the neural activity demonstrated that reported perceptual sensations were better predicted by evoked high gamma power than by stimulation parameters. We then tested the hypothesis that high gamma activation was a marker of perception (independent of stimulus parameters) by testing perception at threshold, where stimulation parameters remained constant but perceptual outcomes differed on a trial-by-trial basis. We found that high gamma power was a consistent and specific biomarker of conscious perception evoked by artificial (electrical) stimuli.

**Results**

For each participant, we chose a single cortical site that had been determined through clinical mapping to evoke a somatosensory percept. We stimulated using a bipolar pair of electrodes at that site spaced 8mm apart to closely replicate the typical clinical stimulation protocol (Fig1A). To determine the effect of stimulation parameters on perception and on neural activity, we employed a 3x3 stimulation pulse train paradigm that included at least five trials each of low (1mA), medium (3-4mA), and high (7-10mA) current amplitudes at frequencies of 10, 50, and 100 Hz. Stimulation pulse trains lasted one second and pulse width was 100us, and were presented in a pseudo-random order. The participants were instructed to push a button with their ipsilateral thumb when and if they felt the stimulation. Electrodes that were responsive to button press in isolation were excluded from further analyses. Across subjects, the proportion of trials that elicited a percept increased, as expected, with increasing charge delivered per unit time (frequency x current, Fig1B).

We next examined the neural recordings associated with stimulation pulse trains in the 3x3 paradigm. To avoid examining data contaminated with stimulation artifact, we analyzed data 100ms following the offset of stimulation. We determined which components of the evoked spectrogram were significantly different from baseline neural data (Fig1C).[22] Across subjects, the only consistent evoked activity in a spectral band that deviated from baseline was a statistically significant increase in the 65-200Hz range, typically referred to as the high gamma range. (z score with respect to baseline distribution, $p<0.01$). The neural frequency of excitation did not vary with stimulation frequency (t-test between average neural responses grouped by stimulation frequency). In a minority of sites, lower frequency bands showed significant deviations from

baseline, but these changes were not consistent across subjects in response to stimulation.

Contrary to our expectations, focal bipolar stimulation was associated with high gamma activation of a relatively large cortical area surrounding the stimulation site. For sites that showed significant high gamma modulation in response to stimulation, the amplitude of their high gamma increase was on average related to their proximity to the stimulation site, but the variability in this relationship was high (Fig 1C, scatterplot). High gamma amplitude versus distance can be approximated by a linear relationship with a negative slope ($R^2$=0.098).

We quantified the time points of significant activity in the high gamma band across patients to determine the typical time course of neural effects following stimulation. Across subjects, two-thirds of significant high gamma increases occurred 100-300ms following stimulation. We therefore defined the time period of 100-300ms as the time period of interest for further analyses.

We used the same methods to quantify the neural response to natural touch in the absence of electrical stimulation (Fig1C, 'Natural touch'). Similarly, natural touch reliably evokes activity above baseline in the high gamma range.

We used a logistic regression across patients to quantify the separate effects of stimulation amplitude and frequency on the probability of causing a conscious percept (Figure 1D). Both increased amplitude and increased charge per time were associated with higher rates of reported perception ($p<10^{-4}$ and $10^{-6}$, respectively). Some parameter combinations are likely to produce a threshold response, where the patient feels the stimulation on approximately half of the trials. Interestingly, at threshold parameter

combinations, we noted increased high gamma activity for perceived trials over non-perceived trials (Fig1D inset).

To test whether high gamma increase and conscious perception are consistently concurrent, we compared perceptual reports with average high gamma activity at sites that modulated their activity in response to stimulation (Fig2A). We found a pronounced co-occurrence of perceptual reports with increased high gamma, and a significant shift to higher high gamma activity for perceptual trials over non-perceptual trials in the 3x3 paradigm (Fig2B).

Perceptual trials co-occur with pulse trains of high stimulation amplitude, high stimulation frequency, or a combination of the two. We next wanted to understand whether the charge delivered, the stimulation frequency, or the stimulation amplitude best correlated with perception. We expanded our 3x3 table of stimulation frequencies and amplitudes so that there was more continuity in tested levels of frequency and amplitude, and so that there were matched pairs of charge per time for a single subject (e.g. 10 Hz at 7.5 mA and 50 Hz at 1.5 mA, both of which inject 75 Hz x mA of charge; matched pairs are outlined in black in Fig2C). In some cases, equal amounts of charge per time are injected, yet the perceptual outcomes are different. There are even examples of the inverse relationship, in which a higher charge per time resulted in fewer positive percepts. For instance, at 100Hz and 3mA ([300 Hz x mA]) the subject in Fig2C felt the stimulation in approximately 20% of the trials, yet at 30Hz and 6mA ([180 Hz x mA]), the subject felt the stimulation in 100% of trials. These differences in outcome from matched pairs of charge illustrate that it is not simply the amount of charge injected per time that leads to a percept. Nor is it solely the stimulation frequency or stimulation

amplitude. Increasing stimulation parameters boosts the chance of evoking a conscious percept, but the stimulation parameters themselves are not the sole determinants of the perceptual outcome of stimulation.

We have shown that increasing stimulation parameters are correlated with high gamma activation. We have also shown that high gamma is associated with perception. As a result, we next wanted to determine whether conscious perception was more dependent on the stimulation parameters or the high gamma activation. We evaluated the best predictors of high gamma change, and whether they differed by cortical site. We employed a series of linear regressions for each cortical site that showed significant high gamma activity above baseline. We predicted high gamma activity following stimulation for each electrode on single trials using frequency, current, charge per time, or percept as sole predictors. We compared the model fits to each other and to a full model that incorporated all of the factors (Fig2D). With only one predictor, we found that for the majority of electrodes, whether or not the stimulus was perceived was the best indicator of high gamma activity. Furthermore, for most electrodes, the model based on percept alone did approximately as well as the full model that included the stimulation parameters and charge per time (mean increase in adjusted $R^2$ was 0.018. Perception predicts high gamma with the same accuracy as perception with all other stimulation parameters (the full model was not significantly different from that of the percept model, p=0.56). Finally, we used an LDA classifier to predict whether the subject perceived the stimulation based on either charge per time or high gamma activity across all significant sites (Fig2E). We found that more trials were accurately classified using high gamma activity than charge per time (93% versus 78%). Across these different methods of

analysis, we determined that the cortical high gamma response to stimulation predicts perception more accurately than stimulation parameters alone.

We now have shown that high gamma activation is a better predictor of stimulation outcome than the stimulation parameters. The ultimate test of this point is the case of threshold stimulation, a paradigm in which stimulation parameters are held constant at a level for which the subject sometimes perceives the stimulation and sometimes does not. Because the stimulation current and frequency are held at the same value for all trials, any consistent differences in the recorded neural signal are necessarily differences in the underlying neural activity and are not from external factors such as stimulation parameters or stimulation artifact.

Up to this point, we have limited our analysis to evoked neural signals following electrical stimulation, to avoid the concern of stimulation artifact during stimulation pulses. Threshold trials enable us to confidently estimate the differences in high gamma signal between perceptual and non-perceived trials during stimulation, since once again the electrical stimulus is identical for both conditions. We employed two complementary techniques to examine high gamma activity during stimulation. The Lomb-Scargle algorithm[23,24] estimates power of a series with missing data points and was used to compare the mean high gamma activity during stimulation at each electrode. The second method, blanking with interpolation, allowed us to examine the time course of the high gamma activity during stimulation at each electrode. The results of the two methods corroborate each other to show that high gamma activity increases during stimulation for perceived trials versus non-perceived trials (Fig3 inset).

Many more electrodes in the vicinity of the stimulation site show increased HG during perceived trials as compared to non-perceived trials at threshold stimulation parameters (Fig 3B). The time course of high gamma activity for perceived versus non-perceived trials shows an increase in the high gamma activation immediately at the start of stimulation that persists during stimulation (Fig3C, $p<0.05$). There is a trend toward higher high gamma in the time period of 100-300ms following stimulation, as we have examined before, but it is not particularly robust for this subset of electrodes. This suggests that some sites respond with high gamma increase during stimulation but not after, while some respond with increased high gamma both during and after the stimulation pulse train. Across patients, normalized high gamma amplitude during stimulation is higher in perceived trials over non-perceived trials (Fig3D, paired t-test, $p=0.0098$).

**Discussion**

Understanding the effects of epicortical stimulation is instrumental to the interpretation of both clinical and scientific studies that employ stimulation in assigning functions to cortical areas. In this study, we used clinically relevant stimulation parameters to evoke sensory perception while measuring the neural response at sites surrounding the stimulation site. Several experimental features enabled us to draw conclusions about effective cortical stimulation on the macro scale. In contrast to other cortical stimulation studies, we were able not only to record neural activity throughout stimulation using a high dynamic range amplifier, but also to densely sample this activity

over centimeters of cortex directly adjacent to the stimulation site. This broad coverage at high density permitted us to determine that there are indeed widespread neural effects of stimulation, while the ability to record through and directly following stimulation allowed us to parse stimulation artifact from real neural modulation. The 3x3 experimental design facilitated our drawing conclusions about the effects of stimulation parameters on both behavioral outcome and neural correlates. Finally, the threshold level stimulation experiments made it possible for us to confidently estimate neural differences during stimulation.

We have shown that: 1) DES evokes neural activity primarily in the high gamma frequency range, 2) high gamma increases in response to stimulation are found beyond the focal site of stimulation to include surrounding cortical regions, 3) high gamma activation above baseline occurs for stimulation that evokes conscious perception, and 4) high gamma increases during stimulation predict conscious sensory perception at threshold stimulation levels. These responses were evident across participants and over many different sites in somatosensory cortex.

The characteristic increase in high gamma following stimulation that we found here is consistent with animal work describing increased neural firing in reaction to electrical microstimulation using pulse trains.[25] Activity in the high gamma range in response to natural stimuli has been observed in sensory cortices dating back decades[26–35], and it was explicitly distinguished from lower frequency bands in studies of human subjects using ECoG.[36,37] It has since proven to be a strong correlate of sensory, motor, and cognitive events.[21,22,36,38–41] High gamma activity correlates well not only with the functional magnetic resonance imaging blood-oxygen level-dependent signal[42–44], but

also with multi-unit firing rate[45], making it a reasonable proxy for evoked neural firing in response to stimulation.

Although the high gamma increase in response to stimulation may be expected in light of these associations, it is important to note the novelty and importance of performing this study using DES. Microstimulation and DES are often incorrectly assumed to induce similar effects and to have comparable behavioral consequences, when in fact, the stimulation parameters, the electrode type, the depth of stimulation into the cortex, and particularly the scale of stimulation differ drastically between the two methods.[17] Because of the clinical relevance of DES and how little we currently understand about its neural effects, it is premature to assume that the same neural mechanisms observed using microstimulation translate to DES.

In a similar way, this work should be distinguished from other studies that use DES electrodes to examine functional connectivity.[46,47] These studies use very low frequency pulses to evoke cortico-cortical evoked potentials (CCEPs). CCEPs provide information solely on network connectivity and are not related to function; they are generated whether or not the stimulation elicits a percept. In contrast, a train of pulses, as used in this study, drives the network, presumably eliciting an integrated response.[17]

The high level of connectivity of the cortex is evident in the responses generated by pulse trains, as evidenced by the broad spatial spread of high gamma responses following stimulation. Other studies have noted CCEPs centimeters away from the stimulation site[46,47], so it is not surprising that in driving cortical activity with DES we observe responses both near and far from the origin of stimulation. The spatial localization of DES has been reported to be 5mm based on function alone.[48] Resulting

neural activation may appear to cover a broader expanse (centimeters as opposed to millimeters) due to the interconnectivity of the stimulated site with other sites in the surrounding area.

Charge delivered per unit time was thought to be the most relevant factor in whether stimulation exceeds threshold for a sensory percept. One example of this comes from microstimulation studies in rats, where it was shown that higher frequency and lower current may be used to achieve a similar sensation as lower frequency and higher current.[49,50] Equivalent charge per time elicited different likelihoods of perception in our subjects, showing that frequency and amplitude may be tuned to deliver the same charge per time but affect perception differently. For instance, a high frequency, low current stimulus may safely achieve the desired outcome without causing the damage to neural tissue that is associated with high currents. This knowledge is useful for achieving adequate stimulation levels while preserving the integrity of neural tissue in long-term devices.[51–53]

Initial experiments revealed activation above baseline following perceived trials, but it was originally unclear whether this reflected perception alone or simply increasing network excitation due to higher stimulation frequency and current. By employing highly controlled threshold stimulation trials, we were able to separate the neural correlates of perception from the correlates of stimulation parameters. We found that both at individual sites and on average, high gamma amplitude is increased during perceived trials over non-perceived trials. Interestingly, the distinction begins at the very start of stimulation, suggesting that the trial is almost immediately classified as one that will be consciously perceived or not. This rapid response is consistent with high gamma being

the intermediary neural signal by which DES causes conscious perception.[54] In addition, it was not previously known whether pulse trains induce or inhibit activity[16]; this study shows that high gamma activity is increased during stimulation at sites surrounding the stimulation site.

Reliable biomarkers of effective stimulation are critical for neural devices that rely on a biofeedback loop. We found that high gamma activation is a reliable biomarker of stimulation that produces a percept in sensory cortex. It is possible and even probable that DES induces high gamma activation irrespective to which brain region it is applied. If this were the case, high gamma could be the biomarker of choice for effective stimulation levels. This would be especially useful for disorders in which there is no expected immediate behavioral outcome, such as mood disorders or learning disorders. Future work can determine whether high gamma as a biomarker is as robust in other areas of cortex, and more specific studies can reveal whether the neural subpopulations that generate the high gamma signal are excitatory, inhibitory, or a mixture of the two.

**Acknowledgements**

The authors would like to thank Dr. Joseph O'Doherty for helpful discussion.

**Online Methods**

*Participants*. Experimental procedures were approved by the Committee for Human Research at the University of California, San Francisco, and all participants provided written informed consent. Patients undergoing ECoG grid implantation for epilepsy focus localization (N=10, 6M/4F, 20 – 55 years old) volunteered to participate in this

research study (Supplementary Table 1). Patients were implanted with 256 channel high-density subdural electrode arrays (AdTech, Racine, WI or Integra, Plainsboro, NJ) with 4mm center-to-center spacing (1.17mm exposed diameter). Electrode arrays were positioned purely according to clinical indications. Participants were included whose coverage included the ventral sensorimotor cortex (pre- and post-central gyri). An electrode in the sub-galeal space served as the reference electrode and ground for recording.

*Tasks and stimuli*. A neurologist (VR or RCK) operated a clinical bipolar stimulator (Natus, XXXX) while monitoring ECoG signal for electrical abnormalities throughout testing. Stimulation pulse train parameters were as follows: biphasic, cathode-leading, pulse width=100 μs, duration = 1sec. In a typical experimental session, the clinician tested several bipolar pairs individually by stimulating with typical clinical parameters and asking the subject to report any sensations evoked by electrical stimulation. The site that produced the most discrete sensory percept was chosen as the test site for the rest of the experimental session. Most of these sites produced percepts in the hand or lower face areas. The subject was instructed to press a button when they felt the percept and to not move otherwise. The subject did not know when stimulation was occurring, as they could not see the operator and there was no sound associated with stimulation. The typical 3x3 table of parameters was then tested with at least five repetitions of stimulation pulse trains for each current and frequency combination. Because the testing would have taken too long if the clinician had changed the parameters for each trial, the five repetitions were always completed back to back. However, each patient had a pseudorandom order of presentation of the current and

frequency combinations. Pulse trains were presented by the operator with several seconds between pulse trains. Across patients, the timing of button press was well-correlated with timing of stimulation pulse trains, and false positives were rare. For the fifty-fifty paradigm, the subject was again instructed to press the button when he or she felt the percept. A mid-range level of current delivered at 50Hz was chosen for testing and titrated until the experimenter determined that the patient was perceiving the stimuli approximately half of the time.

*Button press control*

The subjects were instructed to press the button using their ipsilateral thumb. A button press control task was performed by the subject in the absence of electrical stimuli. The subject was cued by the researcher to press and hold the button. The same statistical analysis that was used to test for increased high gamma following stimulation pulse trains was used to test for high gamma activity over baseline corresponding with the button press. These electrodes were then excluded from further analyses (n=107 of 1824 total electrodes across patients).

*Sensory control*

The sensory control task was performed in the absence of electrical stimuli. In anatomical locations for which it was feasible, the researcher applied light tactile pressure to the anatomical area in which the subject reported feeling paresthesias. The sensory control was time aligned using a corresponding button press by an observing researcher. Because this control was used only to identify the location of neural

representation of the sensory area in question, the exact pressure applied was not analyzed. The same statistical analysis that was used to test for increased high gamma following stimulation pulse trains was used to test for high gamma activity over baseline corresponding with the sensory stimulus. Electrodes that displayed high gamma activity above baseline were then designated as part of the natural sensory network.

*Recording and data processing*

Signals were acquired at a sampling rate of 3051.8 Hz and were amplified and digitized using a Tucker-Davis Technologies (Alachua, FL, USA) neural recording system (RZ2 DSP combined with a 256-channel PZ2 amplifier). Manual artifact and channel rejection was performed, followed by common median referencing.

The signal from each electrode channel was filtered into 40 frequency bands using an FFT followed by a Hilbert transform with logarithmically increasing center frequencies (range of CF = 4.07 Hz – 193.8 Hz). The analytic amplitude, also known as the envelope, and the phase were calculated for each [55]. The high gamma analytic amplitude was calculated by averaging filtered frequencies between 70 and 150 Hz. A z-score of the filtered frequencies was calculated with respect to a rest block recorded during the same session by following the method of Canolty, et al.[22] The anatomical location of electrodes was determined with the aid of co-registered brain CT and MRI images.

*Analytical methods*

To avoid contamination by stimulation artifact, we excluded 100ms of data on either side of the stimulation pulse train. Due to forward and reverse filtering, any artifact from the stimulation is symmetrical at the onset and offset of stimulation. This interval was adequate for artifact rejection for all parameters used, as determined by comparison of z-scored signals prior to stimulation and following stimulation across stimulation parameters, and was corroborated by visual inspection.

The stimulating channel pair was excluded from analyses. Z scored signals were tested for significance from baseline and corrected for false discovery rate using the method of Canolty et al.[22] It was found that the only consistent signal across subjects that differed from baseline was the increased amplitude of the high gamma band following stimulation. The time course of high gamma increase was determined by counting the number of significant timepoints in the high gamma range of the neural spectrogram from 0.1 to 2 seconds post pulse train. In the typical case of high gamma activation across all electrodes, over two thirds of the significant time points occurred in the time period between 0.1 and 0.3 s following stimulation. Thus, the average high gamma power during this time frame is used for following analyses.

*Logistic regression on behavior*

A logistic regression with interactions and random effects by subject was performed with inputs of stimulation frequency and amplitude to predict perception as a binary value. The random effects grouped by subject allowed the subjects to have different intercepts, relating to varying thresholds for perception.

*Linear regression on HG amplitude*

A linear regression was performed for each electrode for the single subject that was able to complete most of a 5x4 matrix of stimulation parameter values (current values of 1.5, 3, 4.5, 6, 7.5mA and frequencies of 10, 30, 50, and 100Hz). This extended matrix of parameters was tested because in this rare case the team had more time to collect data prior to the patient's surgery. This afforded an opportunity to determine what factors best predict increases in high gamma amplitude, and whether there exist subpopulations of electrodes that respond to some parameters and not others. Parameters that went into the regression were frequency, current, charge per time defined as frequency multiplied by current, percept as a 0 or 1, and a full model with all predictors included. Electrodes that never displayed an adjusted $R^2$ of 0.1 or over were discarded from the analysis. Two additional outliers with abnormally high $R^2$ values were identified and removed.

*LDA classification of perceived trials*

For each stimulation parameter pair, a classifier was used to predict whether a conscious percept was elicited with those parameters. In one model, the stimulation frequency, amplitude, and charge per time were the predictors. In the other model, the mean high gamma z score from 100 to 300ms post pulse train for all significant electrodes were the predictors. The classifier was trained on data from all parameter sets except two, and attempted to predict the percept on held out data. The same paradigm was then repeated over 100 iterations to define distributions for the accuracy of stimulation parameters and of high gamma in predicting perception. The result of

each model was a percent correct over all predictions, obtained by dividing the number correct by the total number of predictions.

*Testing for differences between HG traces at threshold*

For data during stimulation, a student's T test was performed on power estimates of high gamma amplitude for each trial obtained with the Lomb-Scargle algorithm. Electrodes with p-values $<0.05$ were noted as significantly different and their T-statistic is shown in Fig3B.

**Code availability**. Custom Matlab scripts were used for analyses in this study. These are available upon reasonable request.

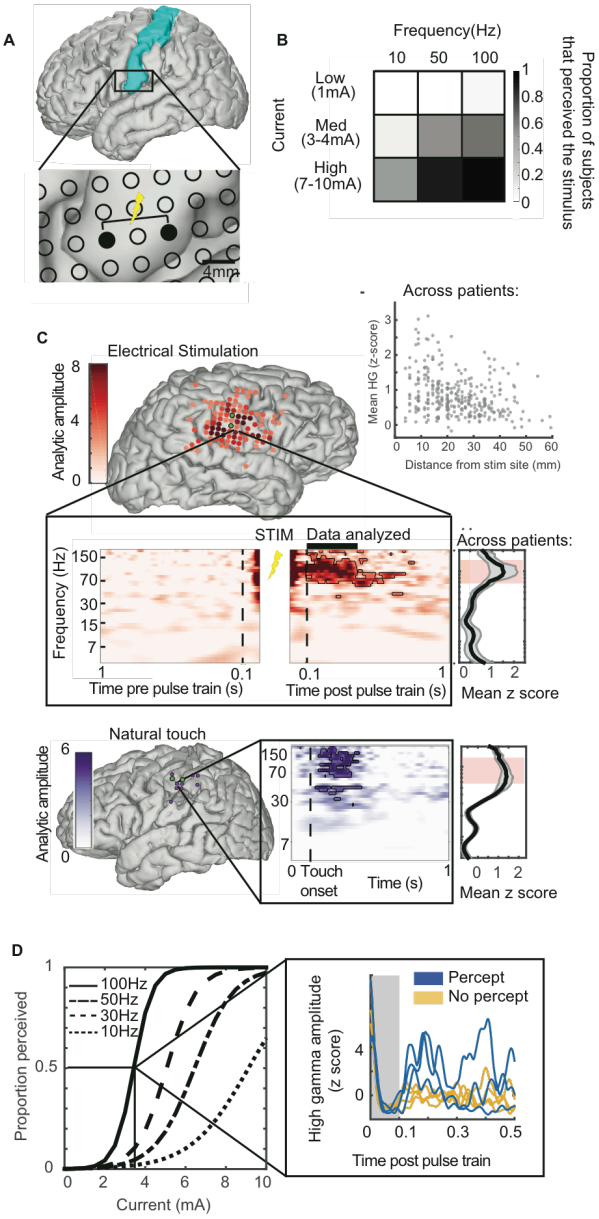


Figure 1: DES causes high gamma (HG) activation following stimulation that elicits conscious perception. A) Somatosensory cortex (highlighted in blue) is the target site of stimulation for all patients. Inset: Bipolar stimulation occurs across two electrodes spaced 8mm apart. Neural activity is recorded throughout the experiment from electrodes surrounding the stimulation site. Recording electrodes are spaced 4mm center-to-center. B) Proportion of subjects that perceived stimulation at each of the nine stimulation parameter combinations. C) Mean HG activation 100-300ms post pulse train is mapped onto the cortical surface for an example subject following stimulation with a parameter set in which the subject reported feeling a percept. Stimulation electrodes are shown in green. Inset: neural spectrogram 1 second before and after stimulation for an example electrode. Neural frequency is on the y-axis in log space. Dashed lines mark 100ms on either side of the stimulation pulse train, denoting the conservative window of time (buffer) that was discarded from analyses to avoid spectral bleed from stimulation artifact. Data points that were determined to be significantly different than baseline activity are outlined in black, and the vast majority of these points appear in the range of 60-150Hz. Right panel: The amplitude during the time window of 100-300ms after stimulation is averaged across electrodes and across patients and shown as the dark black line, with the standard error of the mean in light gray. Red shaded region demarcates the high gamma range. Above: Scatterplot shows mean high gamma versus distance from stimulating pair for each significant electrode across 7 patients. The high gamma amplitude 100-300ms post stimulation offset determines significant electrodes. Natural touch: Electrodes that significantly respond to natural touch are shown on the brain of an example subject in purple, with respect to stimulation electrodes in green. Inset shows the neural spectrogram of an example electrode with respect to onset of natural touch, averaged over 10 trials. Right panel: The amplitude after touch is averaged across electrodes and patients and shown as the dark black line, with the standard error of the mean in light gray. Red shaded region demarcates the high gamma range. D) Logistic regression best-fit lines across patients are shown for each frequency of stimulation as a function of increasing current. Inset: Single trials of HG post pulse train are shown for an example electrode. 0-100ms post offset is shown in gray. To avoid stimulation artifact contamination, this part of the data is not included in analyses. Perceived trials are blue lines, and non-perceived trials are yellow lines.

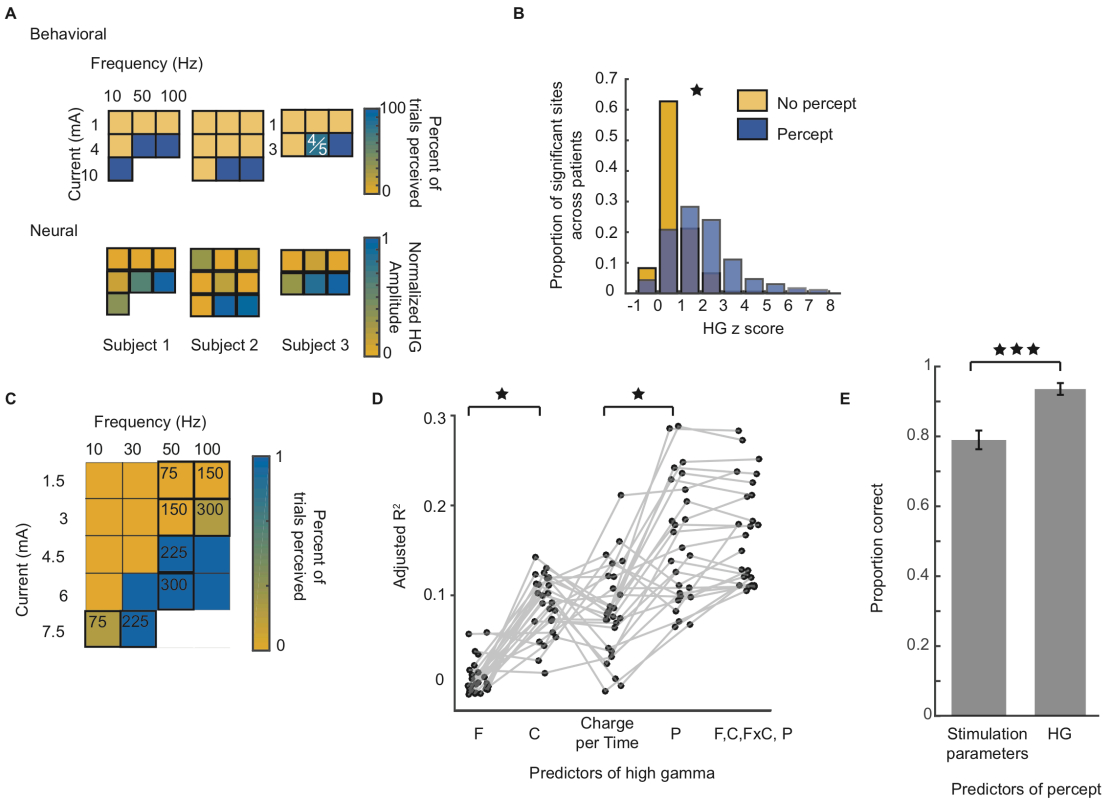


Figure 2: High gamma (HG) amplitude surpasses stimulation parameters in predicting perception. A) Behavioral and neural data are shown for 3 example subjects. Although the goal was to obtain behavioral and neural data for a full 3 x 3 parameter set, some participants did not tolerate the higher stimulation intensities. At least five trials of each stimulation parameter pair were completed. Dark blue boxes indicate that the subject reported feeling the stimulus 5/5 or 100% of the trials unless otherwise noted by text in white. Yellow boxes indicate that the subject reported feeling the stimulus 0/5 trials. For the corresponding neural data, each box denotes a post-stimulus HG z score averaged over electrodes that showed significantly different activity from baseline in the HG band for any stimulation parameter pair, perceived or not. B) Across subjects, the HG z score of significant electrodes shows a shift toward higher values for perceived trials (the two distributions have significantly different means, $p<0.05$ in a paired t-test). C) An expanded experimental paradigm and its corresponding number of trials perceived are shown for one subject where additional stimulation parameters could be tested. Matched pairs of total charge within the extended matrix are outlined and denoted by their total charge (mA x Hz). D) Adjusted R2 values for linear regressions predicting HG amplitude are shown for significant electrodes. Predictors are frequency (F), current (C), charge per time (CT), percept (P, input as 0 or 1), and a full model with all parameters (F,C,FxC,P). Filled dots are adjusted R2 values for each electrode, predicted by the parameter(s) above which they are centered. Gray lines connect the dots to denote the trajectory of the model fit for the same electrode predicted in each of the 5 cases. Neighboring groups were tested pairwise for differences in their means. Stars and brackets demarcate neighboring groups that show a significant difference (Student's t-test, $p<0.0125$). E) LDA classification results for predicting perception at each stimulation parameter pair, bootstrapped over 100 iterations. Gray bars show the relative performance of stimulation parameters and HG across all electrodes above baseline as inputs to the classifier. HG predicts perception better than stimulation parameters of frequency, charge per time, and current (student's t-test, $p<10\text{-}5$).

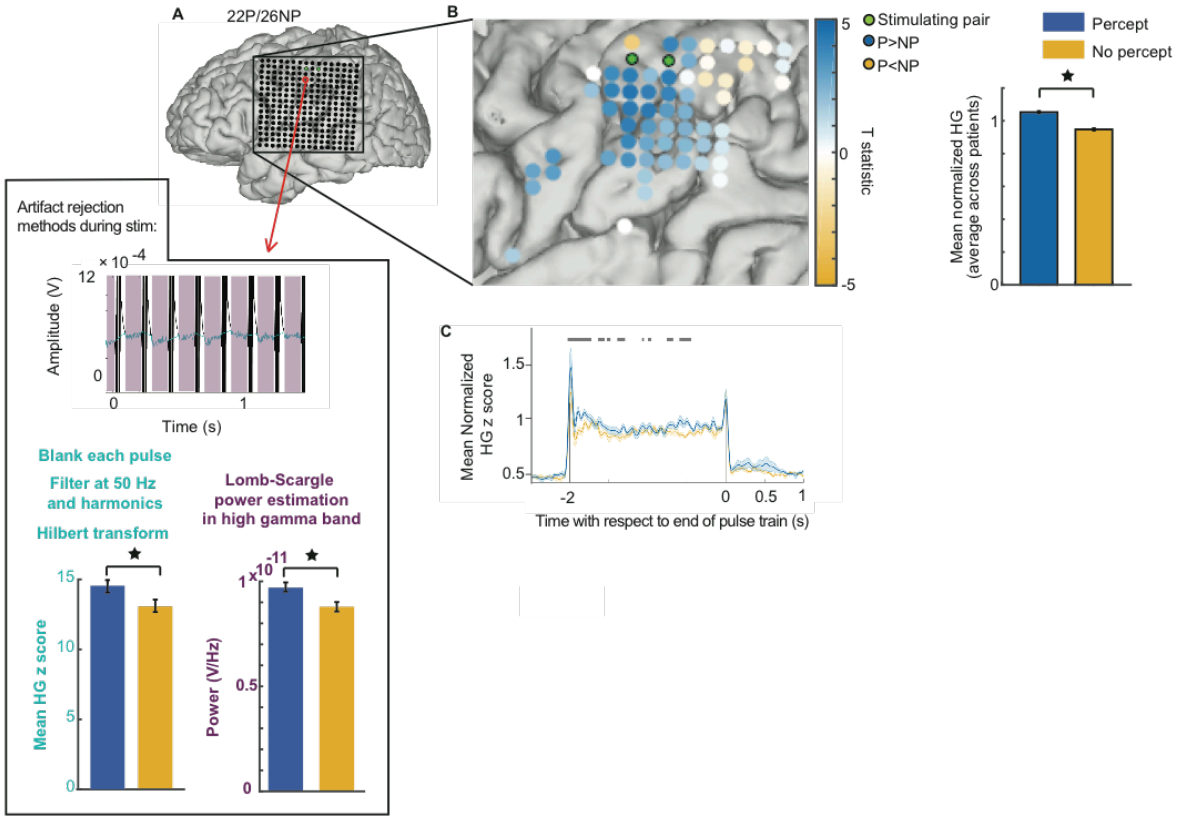


Figure 3: With stimulation parameters held constant, high gamma (HG) amplitude increases on perceived trials, as compared to non-perceived trials. A) 3D MRI brain reconstruction with electrode array placement and stimulating pair is shown for one example subject who was stimulated with threshold level stimulation for 48 stimulation pulse trains. 22 were perceived and 26 were not perceived. Inset: Complementary artifact rejection methods for start and during stimulation. Raw data is shown for an example electrode. It is analyzed using the Lomb-Scargle method over purple highlighted boxes and alternately by using linear interpolation (teal line) followed by Hilbert transform. Bar graphs show that for each artifact rejection method, the result is that high gamma is higher for percept trials over no percept trials during stimulation. B) The T statistic is plotted for each electrode that increased its activity at least 2 standard deviations above baseline during stimulation. A positive T statistic (blue electrodes) denotes that the mean HG power during stimulation was higher in the case of perception over no perception (t-test on Lomb-Scargle processed data). C) Average HG z-score over time is shown for percept and no percept trials. The blue line is the mean HG z-score for perceived trials, and the yellow line is the mean HG z score for non-perceived trials. Shading represents the standard error of their mean across trials, respectively. Gray bar above traces indicates time points that showed a significant difference in high gamma between percept and no percept trials (t-test, $p<0.05$). D) The mean normalized HG during stimulation is shown for percept versus no percept trials (mean across electrodes and subjects). Across subjects, electrodes display significantly higher high gamma amplitudes during stimulation for perceived trials over non-perceived trials (paired t-test, $p=0.0098$).

REFERENCES


1. Penfield, W. & Boldrey, E. Somatic Motor and Sensory Representation in the Cerebral Cortex of Man as studied by Electrical Stimulation. *Brain* (1937).
2. Penfield, W. & Rasmussen, T. The Cerebral Cortex of Man. A Clinical Study of Localization of Function.pdf. *Academic Medicine* **25,** 375 (1950).
3. Foerster, O. & Altenburger, H. *Elektrobiologische vorg{ä}nge an der menschlichen hirnrinde*. (1934). at <https://books.google.com/books?id=hAFqNQEACAAJ>
4. Purpura, D. P., Pool, J. L., Ransohoff, J., Frumin, M. J. & Housepian, E. M. Observations on evoked dendritic potentials of human cortex. *Electroencephalogr Clin Neurophysiol* **9,** 453–459 (1957).
5. Libet, B. in *Somatosensory System* **2,** 743–790 (1973).
6. Desmurget, M., Bonnetblanc, F. & Duffau, H. Contrasting acute and slow-growing lesions: A new door to brain plasticity. *Brain* **130,** 898–914 (2007).
7. Duffau, H. Acute functional reorganisation of the human motor cortex during resection of central lesions: a study using intraoperative brain mapping. *J. Neurol. Neurosurg. Psychiatry* **70,** 506–13 (2001).
8. Duffau, H. *et al.* Usefulness of intraoperative electrical subcortical mapping during surgery for low-grade gliomas located within eloquent brain regions: functional results in a consecutive series of 103 patients. *J. Neurosurg.* **98,** 764–778 (2003).
9. Duffau, H., Sichez, J. P. & Lehéricy, S. Intraoperative unmasking of brain redundant motor sites during resection of a precentral angioma: Evidence using direct cortical stimulation. *Ann. Neurol.* **47,** 132–135 (2000).

10. Berger, M. S. & Rostomily, A. C. Low grade gliomas: Functional mapping resection strategies, extent of resection, and outcome. *J. Neurooncol.* **34,** 85–101 (1997).

11. Sanai, N. & Berger, M. S. Glioma extent of resection and its impact on patient outcome. *Neurosurgery* **62,** 753–764 (2008).

12. Smith, J. S. *et al.* Role of extent of resection in the long-term outcome of low-grade hemispheric gliomas. *J. Clin. Oncol.* **26,** 1338–1345 (2008).

13. Desmurget, M., Song, Z., Mottolese, C. & Sirigu, A. Re-establishing the merits of electrical brain stimulation. *Trends in Cognitive Sciences* **17,** 442–449 (2013).

14. Selimbeyoglu, A. & Parvizi, J. Electrical stimulation of the human brain: perceptual and behavioral phenomena reported in the old and new literature. *Front. Hum. Neurosci.* **4,** 46 (2010).

15. Winawer, J. & Parvizi, J. Linking Electrical Stimulation of Human Primary Visual Cortex, Size of Affected Cortical Area, Neuronal Responses, and Subjective Experience. *Neuron* 1–7 (2016). doi:10.1016/j.neuron.2016.11.008

16. Borchers, S., Himmelbach, M., Logothetis, N. & Karnath, H.-O. Direct electrical stimulation of human cortex - the gold standard for mapping brain functions? *Nat. Rev. Neurosci.* **13,** 63–70 (2012).

17. Vincent, M. *et al.* The difference between electrical microstimulation and direct electrical stimulation - Towards new opportunities for innovative functional brain mapping? *Rev. Neurosci.* **27,** 231–258 (2016).

18. Parvizi, J. *et al.* Electrical Stimulation of Human Fusiform Face-Selective Regions Distorts Face Perception. *J. Neurosci.* **32,** 14915–14920 (2012).

19. Parvizi, J., Rangarajan, V., Shirer, W. R., Desai, N. & Greicius, M. D. The will to persevere induced by electrical stimulation of the human cingulate gyrus. *Neuron* **80,** 1359–67 (2013).

20. Rangarajan, V. *et al.* Electrical stimulation of the left and right human fusiform gyrus causes different effects in conscious face perception. *J. Neurosci.* **34,** 12828–36 (2014).

21. Crone, N. E. *et al.* Functional mapping of human sensorimotor cortex with electrocorticographic spectral analysis. I. Alpha and beta event-related desynchronization. *Brain* **121 ( Pt 1,** 2271–99 (1998).

22. Canolty, R. T. *et al.* Spatiotemporal dynamics of word processing in the human brain. *Front. Neurosci.* **1,** 185–196 (2007).

23. Lomb, N. R. Least-Squares Frequency-Analysis of Unequally Spaced Data. *Astrophys. Space Sci.* **39,** 447–462 (1976).

24. Scargle, J. D. Studies in Astronomical Time-Series Analysis .2. Statistical Aspects of Spectral-Analysis of Unevenly Spaced Data. *Astrophys. J.* **263,** 835–853 (1982).

25. Butovas, S. & Schwarz, C. Spatiotemporal effects of microstimulation in rat neocortex: a parametric study using multielectrode recordings. *J. Neurophysiol.* **90,** 3024–39 (2003).

26. Ectors, L. Étude De L'Activité Électrique Du Cortex Cérébral. *Arch. Int. Physiol.* **43,** 267–298 (1936).

27. Munk, M. H. & Neuenschwander, S. High-frequency oscillations (20 to 120 Hz) and their role in visual processing. *J. Clin. Neurophysiol.* **17,** 341–360 (2000).

28. Brosch, M., Budinger, E. & Scheich, H. Stimulus-related gamma oscillations in primate auditory cortex. *J. Neurophysiol.* **87,** 2715–2725 (2002).

29. Castelo-Branco, M., Neuenschwander, S. & Singer, W. Synchronization of visual responses between the cortex, lateral geniculate nucleus, and retina in the anesthetized cat. *J. Neurosci.* **18,** 6395–6410 (1998).

30. Herculano-Houzel, S., Munk, M. H., Neuenschwander, S. & Singer, W. Precisely synchronized oscillatory firing patterns require electroencephalographic activation. *J. Neurosci.* **19,** 3992–4010 (1999).

31. Neuenschwander, S. & Singer, W. Long-range synchronization of oscillatory light responses in the cat retina and lateral geniculate nucleus. *Nature* **379,** 728–732 (1996).

32. Cracco, R. Q. & Cracco, J. B. Visual evoked potential in man: Early oscillatory potentials. *Electroencephalogr. Clin. Neurophysiol.* **45,** 731–739 (1978).

33. Goff, G. D., Matsumiya, Y., Allison, T. & Goff, W. R. The scalp topography of human somatosensory and auditory evoked potentials. *Electroencephalogr. Clin. Neurophysiol.* **42,** 57–76 (1977).

34. Cobb, W. A. & Dawson, G. D. The latency and form in man of the occipital potentials evoked by bright flashes. *J. Physiol.* **152,** 108–121 (1960).

35. Lachaux, J. P. *et al.* The many faces of the gamma band response to complex visual stimuli. *Neuroimage* **25,** 491–501 (2005).

36. Crone, N., Boatman, D., Gordon, B. & Hao, L. Induced electrocorticographic gamma activity during auditory perception. *Clinical Neurophysiology* (2001).

37. Edwards, E., Soltani, M., Deouell, L. Y., Berger, M. S. & Knight, R. T. High

gamma activity in response to deviant auditory stimuli recorded directly from human cortex. *J. Neurophysiol.* **94,** 4269–4280 (2005).

38. Mesgarani, N., Cheung, C., Johnson, K. & Chang, E. F. Phonetic feature encoding in human superior temporal gyrus. *Science* **343,** 1006–10 (2014).
39. Cheung, C. & Chang, E. F. Real-time, time–frequency mapping of event-related cortical activation. *J. Neural Eng.* **9,** 46018 (2012).
40. Crone, N. E. *et al.* Electrocorticographic gamma activity during word production in spoken and sign language. *Neurology* **57,** 2045–2053 (2001).
41. Crone, N. E., Miglioretti, D. L., Gordon, B., Lesser, R. P. & Crone, N. Functional mapping of human sensorimotor cortex with electrocorticographic spectral analysis II. Event-related synchronization in the gamma band. *Brain* **121,** 2301–2315 (1998).
42. Mukamel, R. *et al.* Coupling between neuronal firing, field potentials, and FMRI in human auditory cortex. *Science* **309,** 951–954 (2005).
43. Logothetis, N. K., Pauls, J., Augath, M., Trinath, T. & Oeltermann, A. Neurophysiological investigation of the basis of the fMRI signal. *Nature* **412,** 150–157 (2001).
44. Niessing, J. *et al.* Hemodynamic signals correlate tightly with synchronized gamma oscillations. *Science* **309,** 948–951 (2005).
45. Ray, S., Crone, N. E., Niebur, E., Franaszczuk, P. J. & Hsiao, S. S. Neural correlates of high-gamma oscillations (60-200 Hz) in macaque local field potentials and their potential implications in electrocorticography. *J. Neurosci.* **28,** 11526–11536 (2008).

46. Matsuzaki, N., Juhász, C. & Asano, E. Cortico-cortical evoked potentials and stimulation-elicited gamma activity preferentially propagate from lower- to higher-order visual areas. *Clin. Neurophysiol.* **124,** 1290–1296 (2013).

47. Keller, C. J. *et al.* Intrinsic functional architecture predicts electrically evoked responses in the human brain. *Proc. Natl. Acad. Sci. U. S. A.* **108,** 10308–13 (2011).

48. Mandonnet, E., Winkler, P. A. & Duffau, H. Direct electrical stimulation as an input gate into brain functional networks: Principles, advantages and limitations. *Acta Neurochirurgica* **152,** 185–193 (2010).

49. Butovas, S. & Schwarz, C. Detection psychophysics of intracortical microstimulation in rat primary somatosensory cortex. *Eur. J. Neurosci.* **25,** 2161–2169 (2007).

50. Davidovics, N. S., Fridman, G. Y., Chiang, B. & Santina, C. C. Della. Effects of biphasic current pulse frequency, amplitude, duration, and interphase gap on eye movement responses to prosthetic electrical stimulation of the vestibular nerve. *IEEE Trans. Neural Syst. Rehabil. Eng.* **19,** 84–94 (2011).

51. Merrill, D. R., Bikson, M. & Jefferys, J. G. R. Electrical stimulation of excitable tissue: Design of efficacious and safe protocols. *J. Neurosci. Methods* **141,** 171–198 (2005).

52. McCreery, D. B., Agnew, W. F., Yuen, T. G. H. & Bullara, L. Charge density and charge per phase as cofactors in neural injury induced by electrical stimulation. *IEEE Trans. Biomed. Eng.* **37,** 996–1001 (1990).

53. Shannon, R. V. A Model of Safe Levels for Electrical Stimulation. *IEEE Trans.*

*Biomed. Eng.* **39,** 424–426 (1992).

54. Tononi, G. & Koch, C. *The Neural Correlates of Consciousness*. *Ann. N. Y. Acad. Sci.* **1124,** 239–261 (2008).

55. Edwards, E. *et al.* Comparison of time-frequency responses and the event-related potential to auditory speech stimuli in human cortex. *J. Neurophysiol.* **102,** 377–386 (2009).

# Conclusion

In this work we have tackled key aspects of the two major topics that are crucial to building closed loop neural devices: signal recording and electrical stimulation. Using human subjects, we studied the spatial resolution at the cortical surface to decide the necessary and sufficient density of electrodes in different brain regions and for various neural frequency bands. We then designed, fabricated, and tested a device that records signals at even higher density from the surface of a single gyrus, and we found that decoding of brain signals improves with increased density. Finally, we discovered that effective electrical pulse trains are associated with increased high gamma activity during and after stimulation, suggesting that eliciting high gamma activity is the primary mechanism by which stimulation affects neural circuits.

The work presented here will lead to the design of better neural devices, devices that record from large brain areas at sufficient resolution and stimulate one or many nodes in the neural circuitry to reap therapeutic effects. Devices of this sort can provide novel therapies for neuropsychiatric disorders, motor disorders, sensory disorders, and epilepsy.

**Publishing Agreement**

It is the policy of the University to encourage the distribution of all theses, dissertations, and manuscripts. Copies of all UCSF theses, dissertations, and manuscripts will be routed to the library via the Graduate Division. The library will make all theses, dissertations, and manuscripts accessible to the public and will preserve these to the best of their abilities, in perpetuity.

I hereby grant permission to the Graduate Division of the University of California, San Francisco to release copies of my thesis, dissertation, or manuscript to the Campus Library to provide access and preservation, in whole or in part, in perpetuity.

Author Signature Leah Mills

Date May 16, 2017